

# Semiclassical Electron and Phonon Transport from First Principles: Application to Layered Thermoelectrics

Anderson S. Chaves,<sup>1</sup> Michele Pizzochero,<sup>1</sup> Daniel T.

Larson,<sup>2</sup> Alex Antonelli,<sup>3</sup> and Efthimios Kaxiras<sup>1,2</sup>

<sup>1</sup>*School of Engineering and Applied Sciences, Harvard University,  
Cambridge, Massachusetts 02138, United States*

<sup>2</sup>*Department of Physics, Harvard University,  
Cambridge, Massachusetts 02138, United States*

<sup>3</sup>*Gleb Wataghin Institute of Physics,  
University of Campinas, UNICAMP,  
13083-859 Campinas, São Paulo, Brazil*

(Dated: February 2, 2023)

## Abstract

Thermoelectrics are a promising class of materials for renewable energy owing to their capability to generate electricity from waste heat, with their performance being governed by a competition between charge and thermal transport. A detailed understanding of energy transport at the nanoscale is thus of paramount importance for developing efficient thermoelectrics. Here, we provide a comprehensive overview of the methodologies adopted for the computational design and optimization of thermoelectric materials from first-principles calculations. First, we introduce density-functional theory, the fundamental tool to describe the electronic and vibrational properties of solids. Next, we review charge and thermal transport in the semiclassical framework of the Boltzmann transport equation, with a particular emphasis on the various scattering mechanisms between phonons, electrons, and impurities. Finally, we illustrate how these approaches can be deployed in determining the figure of merit of tin and germanium selenides, an emerging family of layered thermoelectrics that exhibits a promising figure of merit. Overall, this review article offers practical guidelines to achieve an accurate assessment of the thermoelectric properties of materials by means of computer simulations.

## CONTENTS

I. Introduction	3
II. Theoretical framework	4
A. Kohn-Sham (KS) Density Functional Theory	4
B. Technical aspects of DFT calculations	6
C. Lattice dynamics from density functional perturbation theory	8
III. Charge and thermal transport	12
A. Justification for the Bloch-Boltzmann formalism	13
B. Boltzmann Transport Equation (BTE)	14
C. Relaxation Time Approximation (RTA)	15
D. Thermoelectric kinetic coefficients tensors	16
E. Scattering mechanisms within semiclassical BTE	18
1. Electron-phonon interaction	18
2. Frölich dipole and quadrupolar el-ph coupling	20
3. Screening for long-range interactions	23
4. Defect scattering	24
5. Phonon-phonon scattering	26
6. Phonon-electron scattering	26
7. Isotope and boundary scattering of phonons	26
8. Combining scattering processes through Mathiessen's rule	27
F. Iterative approach for solving the BTE	27
IV. Numerical approaches and post-processing	28
A. Interpolation schemes	29
B. <code>turboEPW</code> with dual interpolation	30
C. Third order force constants	33
D. Calculating transport coefficients	33
V. Application to layered thermoelectric materials	33
A. Thermoelectric $zT$ optimization	33
B. Electronic transport in SnSe and GeSe	35

C. Thermal transport in SnSe and GeSe	38
D. Thermoelectric figure of merit in SnSe and GeSe	40
VI. Conclusions	42
Acknowledgments	42
References	42

## I. INTRODUCTION

Navigating the global challenges for sustainable energy production, distribution, and use requires continued exploration of new and tailor-made materials to increase efficiency. Detailed knowledge and understanding of electrical and thermal transport properties allows for their optimization, hastening technological development. Since thermoelectric devices can convert waste heat to electricity without any mechanical parts, developing improved thermoelectric materials is a promising approach for energy efficiency and reliability [1].

This paper provides an overview of the first-principles tools that can be used to calculate the transport properties of layered crystal structures. Starting from the density functional theory (DFT) approach to calculating the ground state of the many-body quantum mechanical electron-nuclear Hamiltonian, we describe how various scattering rates, including electron-phonon, phonon-phonon, polar, and defect scattering, can be determined and used as input to the semiclassical Boltzmann Transport Equation (BTE) in order to calculate transport properties such as electrical and thermal conductivity.

To demonstrate the power of this framework we focus on the thermoelectric figure of merit,  $zT$ . Not only is the study and optimization of thermoelectric materials a vibrant and timely research direction due to the importance of thermoelectrics for energy recovery from waste heat, the determination of  $zT = \sigma S^2 T / (\kappa_{\text{carr}} + \kappa_{\text{latt}})$ , requires knowledge of several distinct transport properties that are amenable to first-principles calculations, namely the electrical conductivity  $\sigma$ , Seebeck coefficient  $S$ , carrier (electron or hole) thermal conductivity  $\kappa_{\text{carr}}$ , and the lattice thermal conductivity  $\kappa_{\text{latt}}$ , all for a given temperature  $T$ . A high-level workflow for the calculation of  $zT$  is shown in Fig. 1. Our aim in the following is to give some more detailed explanations of both the conceptual and practical aspects of each of the

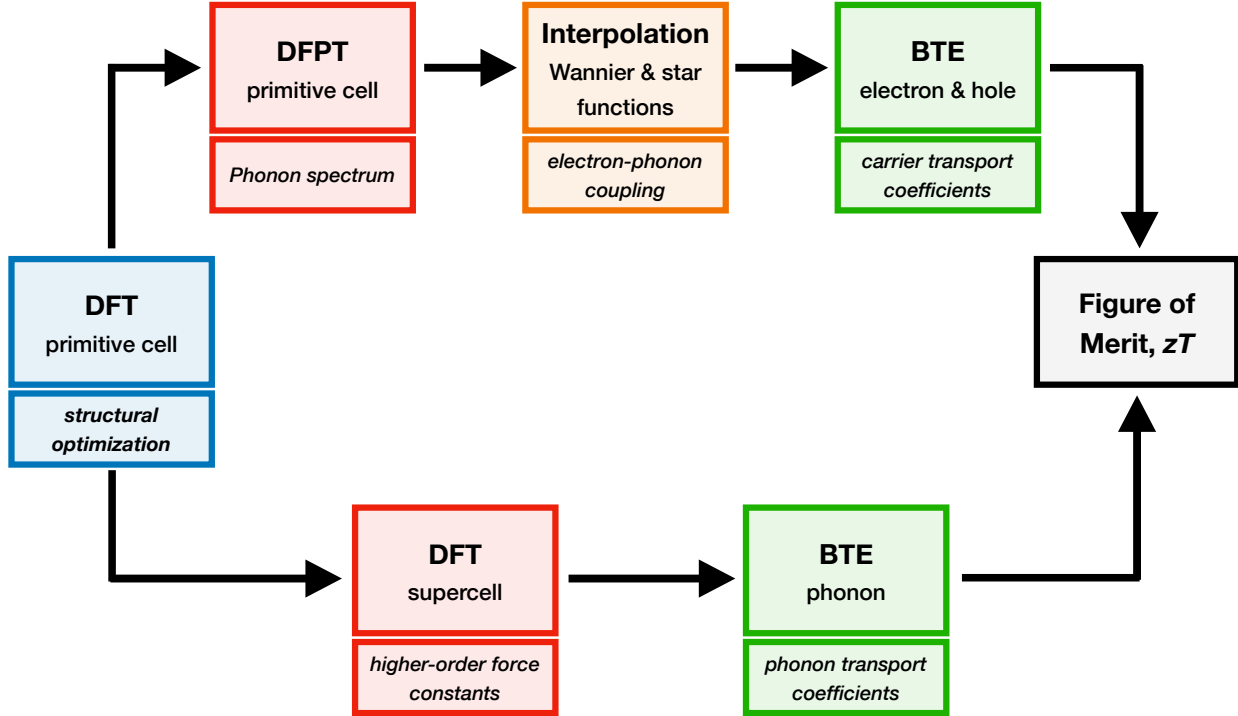


FIG. 1. Computational workflow for the calculation of the thermoelectric figure of merit,  $zT$ , using first-principles methods based on density functional theory (DFT).

steps in the calculation.

The rest of the article is organized as follows. In Sect. II we discuss the basic principles of DFT, the computational tool that underlies these first-principles calculations, and also density functional perturbation theory (DFPT). In Sect. III we present the Boltzmann Transport Equation and describe in detail several important scattering mechanisms. Sect. IV gives details on the post-processing of the DFT results, and Sect. V describes the application of these computational tools in the prediction of  $zT$  for SnSe and GeSe. Finally, we conclude in Sect. VI.

## II. THEORETICAL FRAMEWORK

### A. Kohn-Sham (KS) Density Functional Theory

Owing to the relative simplicity, reliability, reasonable computational effort, and extensive implementation in widely available software packages [2], DFT has rapidly emerged as the method of choice to find approximate solutions to the many-body problem and determine

the properties of molecules and materials at the quantum-mechanical level [3]. DFT is conceptually rooted in the two theorems introduced by Hohenberg and Kohn [4], and its practical deployment follows the KS Hamiltonian [5],

$$\hat{H}^{KS} = -\frac{1}{2}\nabla^2 + V(\mathbf{r}) + V_{\text{H}}(\mathbf{r}) + V^{xc}(\mathbf{r}), \quad (1)$$

where  $V(\mathbf{r})$  is the external potential,  $V_{\text{H}}(\mathbf{r})$  the Hartree potential, and  $V^{xc}(\mathbf{r})$  the exchange-correlation potential. This Hamiltonian leads to a set of  $n$  Schrödinger-like equations for the single-particle Kohn-Sham orbitals  $\Psi(\mathbf{r})$  and accompanying energies  $\epsilon$ ,

$$\hat{H}^{KS}\Psi_i(\mathbf{r}) = \epsilon_i\Psi_i(\mathbf{r}). \quad (2)$$

The solution of the Kohn-Sham equations proceeds in self-consistent fashion by (i) starting with an educated guess of the electron density  $n_k(\mathbf{r})$  to (ii) construct the Kohn-Sham Hamiltonian  $\hat{H}^{KS}$ , (iii) finding upon diagonalization the corresponding eigenvalues  $\epsilon_i$  and eigenvectors, which are subsequently used to (iv) obtain the new density  $n_{k+1}(\mathbf{r})$ , until the difference between  $n_{k+1}(\mathbf{r})$  and  $n_k(\mathbf{r})$  does not exceed a given numerical tolerance.

A number of approximations to the exchange-correlation potential appearing in Equation 1 has been devised [6, 7], most notably (i) the Local Density Approximation (LDA) [8], in which the electron density is assumed to be locally the same as a spatially uniform electron gas with the same density, (ii) the Generalized Gradient Approximation (GGA) [9–12] and Meta-Generalized Gradient Approximation (meta-GGA) [13, 14], where the gradient and Laplacian of the electron density, respectively, are taken into account to increase the accuracy over LDA, and (iii) hybrid functionals [15–17], in which a fraction of the orbital-dependent, exact Fock exchange is included in the otherwise bare GGA.

Although the exchange interactions between electrons can be determined exactly (cf. Hartree-Fock equations), correlation interactions are invariably approximated, a trait that is common to all the exchange-correlation functionals listed above. It is therefore not surprising that density-functional theory provides an inaccurate account of those physical situations where correlation effects dominate, for example, van der Waals interactions or localized electronic states. In addition, being DFT commonly considered a ground state theory (cf. Hohenberg-Kohn theorems), predictions concerning excited states and band gaps are often quantitatively unreliable, see references [18, 19] for through discussions.

## B. Technical aspects of DFT calculations

The computational burden associated with the approximate solution of the Kohn-Sham equation for an  $n$ -electron system can be mitigated by the introduction of pseudopotentials. Core electrons are largely unaffected by the chemical environment and they do not participate in the majority of physico-chemical processes such as chemical bonds or low-energy excitations. Hence, one can replace an explicit single-particle description of core electrons with an effective Coulomb potential. The quality of a pseudopotential is assessed by its transferability, that is, the ability to accurately describe the core electrons of a given element when embedded in different chemical environments. In order to construct a pseudopotential of a chemical element, one has to proceed as follows:

1. Perform an all-electron calculation of the isolated atom and separate the resulting energy levels in core and valence levels according to a threshold. A larger number of valence electrons increases the computational effort, eventually converging to the (exact) all-electron limit, whereas a larger number of core electrons is detrimental to the transferability.
2. Select a core radius,  $r_c$ , such that the valence electron wavefunction of the pseudopotential wavefunction under construction matches the all-electron wavefunction previously calculated beyond  $r_c$ .
3. Construct pseudo-wavefunctions inside the core region. Several methods leading to several flavors of pseudopotentials have been introduced, for instance ultrasoft [20] or norm-conserving [21] schemes.

When core electrons are described through pseudopotentials, one is left with valence electrons, the wavefunctions  $\phi(\mathbf{r})$  of which are expanded on a finite basis. When periodic boundary conditions apply, like in the case of crystalline materials, one can take advantage of the Bloch theorem, which allows the single-particle wavefunctions to be labeled by a band index  $n$  and the crystal momentum  $\mathbf{k}$  and written as the product of a plane wave and a function that is periodic in the crystal lattice:

$$\phi_{n,\mathbf{k}}(\mathbf{r}) = u_{n,\mathbf{k}}(\mathbf{r})e^{i\mathbf{k}\cdot\mathbf{r}}, \quad u_{n,\mathbf{k}}(\mathbf{r} + \mathbf{R}) = u_{n,\mathbf{k}}(\mathbf{r}). \quad (3)$$

Software	License	Reference	Webpage
ABINIT	Free, GPL	[22]	<a href="http://www.abinit.org">www.abinit.org</a>
CASTEP	Academic, Commercial	[23]	<a href="http://www.castep.org">www.castep.org</a>
GPAW	Free, GPL	[24]	<a href="http://wiki.fysik.dtu.dk/gpaw">wiki.fysik.dtu.dk/gpaw</a>
ONETEP	Academic, Commercial	[25]	<a href="http://www.onetep.org">www.onetep.org</a>
Quantum ESPRESSO	Free, GPL	[26]	<a href="http://www.quantum-espresso.org">www.quantum-espresso.org</a>
VASP	Academic, Commercial	[27, 28]	<a href="http://www.vasp.at">www.vasp.at</a>

TABLE I. A list of representative software packages implementing plane-wave DFT for solid-state systems.

Because of this periodicity,  $u_{n,\mathbf{k}}(\mathbf{r})$  can be expanded in a Fourier series including only reciprocal lattice vectors,  $\mathbf{G}$ :

$$u_{n,\mathbf{k}}(\mathbf{r}) = \sum_{\mathbf{G}} e^{i\mathbf{G}\cdot\mathbf{r}} u_{n,\mathbf{k}}(\mathbf{G}). \quad (4)$$

Thus, plane waves are the most natural basis set for periodic systems. According to Eq. (3), however, the evaluation of the solution at a single point requires the summation over an infinite number of  $\mathbf{G}$  vectors. In practice, this expansion is truncated to an energy cutoff,  $E_{\text{cut}}$ , implying that only solutions of kinetic energy

$$\frac{\hbar^2}{2m_e} |\mathbf{k} + \mathbf{G}|^2 < E_{\text{cut}} \quad (5)$$

are evaluated. Delocalized plane waves further offer the advantage of completeness, and the convergence of the calculated properties can be systematically improved by increasing the energy cutoff [29]. A list of representative software packages implementing plane-wave density-functional theory for solid-state systems is given in Table I.

Although extended Bloch orbitals are the most natural choice to describe the electronic states of a periodic system, an alternative approach based on the Wannier representation is convenient for an array of applications in electronic structure [30, 31]. Contrary to Bloch orbitals, Wannier functions provide a real-space representation of localized orbitals which are specified by a lattice vector  $R$  and a band index  $n$ . The general transformation from Bloch orbitals into Wannier functions is

$$|W_{\mathbf{R},n}\rangle = \frac{V}{(2\pi)^2} \int_{\text{BZ}} d\mathbf{k} \sum_{m=1}^N U_{m,n}^{\mathbf{k}} u_{m,\mathbf{k}} e^{-i\mathbf{k}\cdot\mathbf{R}}, \quad (6)$$

where  $V$  is the volume of the primitive cell and  $U_{m,n}^{\mathbf{k}}$  is a gauge-fixing,  $N$ -dimensional unitary matrix. Additional freedom in choice of  $U_{m,n}^{\mathbf{k}}$  means that the Wannier functions are not uniquely determined. A popular choice for the gauge is determined by minimizing the spread functional,  $\Omega$ :

$$\frac{\partial \Omega[U]}{\partial U} = 0, \quad (7)$$

where

$$\Omega = \sum_n \left[ \langle W_{0,n} | r^2 | W_{0,N} \rangle - \langle W_{0,n} | r | W_{0,n} \rangle^2 \right]. \quad (8)$$

Wannier functions obtained following this procedure are referred to as Maximally Localized Wannier Functions (MLWF). Wannierization of DFT calculations is typically performed with the Wannier90 package [32, 33].

### C. Lattice dynamics from density functional perturbation theory

Within the Born-Oppenheimer (BO) approximation, the lattice-dynamical properties of a system can be determined by obtaining the eigenvalues,  $E$ , and the eigenvectors,  $\Phi$ , of the following Schrödinger equation [34]

$$\left( \sum_I \frac{\hbar^2}{2M_I} \frac{\partial^2}{\partial \mathbf{R}_I^2} + \hat{H}_{BO}(\mathbf{R}) \right) \Phi(\mathbf{R}) = E(\mathbf{R}) \Phi(\mathbf{R}). \quad (9)$$

Here, the index  $I$  labels each ion in the system, while  $\mathbf{R}_I$  and  $M_I$  correspond to its coordinates and masses, respectively. For conciseness,  $\mathbf{R}$  correspond to all ionic coordinates and  $\hat{H}_{BO}$  is the BO electronic Hamiltonian that depends parametrically upon  $\mathbf{R}$

$$\hat{H}_{BO}(\mathbf{R}) = \frac{-\hbar^2}{2m} \sum_i \frac{\partial^2}{\partial \mathbf{r}_i^2} + \frac{e^2}{2} \sum_{i \neq j} \frac{1}{|\mathbf{r}_i - \mathbf{r}_j|} - \sum_{iI} \frac{Z_I e^2}{|\mathbf{r}_i - \mathbf{R}_I|} + \frac{e^2}{2} \sum_{I \neq J} \frac{Z_I Z_J}{|\mathbf{R}_I - \mathbf{R}_J|}. \quad (10)$$

Interatomic forces are computed from the derivative of the ground-state energy with respect to the ion positions, and can be calculated by using the Hellmann-Feynman theorem [35, 36]:

$$\mathbf{F}_I = -\frac{\partial E(\mathbf{R})}{\partial \mathbf{R}_I} = -\langle \Phi(\mathbf{R}) | \frac{\partial(\hat{H}_{BO})}{\partial \mathbf{R}_I} | \Phi(\mathbf{R}) \rangle \quad (11)$$

$$= - \int n_{\mathbf{R}}(\mathbf{r}) \frac{\partial V_{\mathbf{R}}(\mathbf{r})}{\partial \mathbf{R}_I} d\mathbf{r} - \frac{E_N(\mathbf{R})}{\partial \mathbf{R}_I}, \quad (12)$$

where  $\mathbf{R}_I = \mathbf{R}_p + \xi_{\kappa} = \mathbf{R}_p + \xi_{\kappa\alpha}$ , with  $\mathbf{R}_p$  one of the direct lattice vectors of a Born-von Kármán supercell composed of  $N_p$  unit cells of the crystal, and  $\xi_{\kappa}$  ( $\xi_{\kappa\alpha}$ ) is the position vector

(with Cartesian coordinate  $\alpha$ ) of the nucleus  $\kappa$  in the primitive unit cell. In Eq. (12) we have

$$V_{\mathbf{R}}(\mathbf{r}) = \sum_{iI} \frac{Z_I e^2}{|\mathbf{r}_i - \mathbf{R}_I|} , \quad (13)$$

which is the external potential, and  $n_{\mathbf{R}}(\mathbf{r})$  is the ground-state electron charge density for a given geometry. Equation (12) assumes the external potential acting on the electrons is a differentiable function of the crystal coordinates. In particular, the equilibrium geometry is reached when forces acting on individual ion vanish, that is,  $\mathbf{F}_I \equiv \frac{\partial E(\mathbf{R})}{\partial \mathbf{R}_I} = 0$ . The vibrational properties of a system can be determined by the interatomic force constants, which correspond to the second derivatives of  $E(\mathbf{R})$  in relation to ion displacements and can be calculated via Hellmann-Feynman theorem as well

$$\mathbf{C}_{\kappa\alpha p, \kappa'\alpha'p'} = \frac{\partial^2 E}{\partial \xi_{\kappa\alpha p} \partial \xi_{\kappa'\alpha'p'}} \quad (14)$$

$$\mathbf{C}_{I,J} = \frac{\partial^2 E(\mathbf{R})}{\partial \mathbf{R}_I \partial \mathbf{R}_J} = -\frac{\partial \mathbf{F}_I}{\partial \mathbf{R}_J} \quad (15)$$

$$= \int \frac{\partial n_{\mathbf{R}}(\mathbf{r})}{\partial \mathbf{R}_J} \frac{\partial V_{\mathbf{R}}(\mathbf{r})}{\partial \mathbf{R}_I} d\mathbf{r} + \int n_{\mathbf{R}}(\mathbf{r}) \frac{\partial^2 V_{\mathbf{R}}(\mathbf{r})}{\partial \mathbf{R}_I \partial \mathbf{R}_J} d\mathbf{r} + \frac{\partial^2 E_N(\mathbf{R})}{\partial \mathbf{R}_I \partial \mathbf{R}_J} , \quad (16)$$

where  $\frac{\partial n_{\mathbf{R}}(\mathbf{r})}{\partial \mathbf{R}}$  is the linear response of  $n_{\mathbf{R}}(\mathbf{r})$  to a distortion of the nuclear geometry, which is a fundamental result derived by De Cicco and Johnson [37] and by Pick, Cohen, and Martin [38]. This establishes that, within the adiabatic approximation, the electrons feel only a static phonon perturbation. It is important to note that, due to translational invariance, the interatomic force constants depend on  $p$  and  $p'$  only through the difference  $\mathbf{R}_p - \mathbf{R}_{p'}$ . The Fourier transform of the interatomic force constants

$$D_{\kappa\alpha, \kappa'\alpha'}(\mathbf{q}) = \frac{1}{\sqrt{M_\kappa M_{\kappa'}}} \sum_p \mathbf{C}_{\kappa\alpha 0, \kappa'\alpha'p} e^{i\mathbf{q}\cdot\mathbf{R}_p} , \quad (17)$$

is the (hermitian) dynamical matrix [39], where  $M_\kappa$  is the mass of the ion  $\kappa$ . Because of the translational invariance, the lattice distortion is monochromatic, meaning that a phonon perturbation with wavevector  $q$  does not induce a force response with wave vector  $\mathbf{q}' \neq \mathbf{q}$ . The phonon eigenfrequencies of the phonon mode  $\nu$  and wave vector  $\mathbf{q}$ ,  $\omega_{\nu\mathbf{q}}$ , are obtained by diagonalizing the dynamical matrix

$$\sum_{\kappa'\alpha'} D_{\kappa\alpha, \kappa'\alpha'}(\mathbf{q}) e_{\kappa'\alpha', \nu}(\mathbf{q}) = \omega_{\nu\mathbf{q}}^2 e_{\kappa\alpha, \nu}(\mathbf{q}) , \quad (18)$$

and the eigenvectors  $e_{\kappa'\alpha', \nu}(\mathbf{q})$  are the phonon polarizations.

We now briefly introduce density functional perturbation theory (DFPT), which can be used to calculate the interatomic force constants and vibrational spectra as well as the electron-phonon matrix elements. As presented in the last section, DFT allows for the calculation of the total energy and charge density, which can in turn be used to obtain a large number of experimental observables. DFPT allows one to obtain quantities that depend on derivatives of the total energy and charge density with respect to a small change in the potential. Even though they can also be obtained through finite difference approaches, DFPT is often more powerful because it does not require large supercells and can be calculated for perturbations of any wavelength, enabling the calculation of different properties in condensed matter physics such as vibrational frequencies, elastic constants, dielectric tensors, Born effective charges, piezoelectric tensors and flexoelectricity [40–49].

First-order perturbative approaches within DFT were proposed independently by different groups working in different contexts [50–55]. Specifically, the investigation of perturbations in condensed matter physics, such as the response of fermionic systems to displacement of atoms within DFT, has been pioneered by Zein [54], Baroni, Giannozzi and Testa [55], and Gonze [56]. A generalization to arbitrary order was introduced by Gonze and Vigneron [57], on the basis of the  $2n + 1$  theorem of perturbation theory [58]. Such perturbative approaches are based on different techniques comprising Green’s functions [55], the generalized Sternheimer equation [52, 59], or the Hylleraas variational scheme [60, 61]. Below we will follow the generalized Sternheimer approach. Connections to other techniques have been discussed extensively elsewhere [60].

Equation 14 demonstrates that the matrix of force constants are determined by the electron-density linear response,  $\partial n$ . Here we will write the KS eigenfunctions  $\Psi_{n\mathbf{k}}$  in the Bloch form

$$\Psi_{n\mathbf{k}}(\mathbf{r}) = N_p^{-1/2} \psi_{n\mathbf{k}}(\mathbf{r}) e^{i\mathbf{k}\cdot\mathbf{r}}. \quad (19)$$

with lattice periodic part  $\psi_{n\mathbf{k}}$ . The density  $n$  is given by

$$n(\mathbf{r}) = \sum_{n\mathbf{k}} |\Psi_{n\mathbf{k}}(\mathbf{r})|^2 \quad (20)$$

where the band index  $\nu$  indicates occupied states only. Within DFPT,  $\partial n$  is induced by the first-order variation of the KS potential,  $\partial_{\kappa\alpha,\mathbf{q}} v^{KS}(\mathbf{r}) e^{i\mathbf{q}\cdot\mathbf{r}}$ , and can be calculated through the

first-order variation of the lattice periodic KS wave functions,  $\partial\psi_{n\mathbf{k},\mathbf{q}}e^{i\mathbf{q}\cdot\mathbf{r}}$ :

$$\partial n_{\kappa\alpha,\mathbf{q}}(\mathbf{r}) = \frac{2}{N_p} \sum_{\nu\mathbf{k}} \psi_{\nu\mathbf{k}}^* \partial\tilde{\psi}_{\nu\mathbf{k},\mathbf{q}}. \quad (21)$$

In Eq. (21),  $\partial\tilde{\psi}_{\nu\mathbf{k},\mathbf{q}} = P^c \partial\psi_{\nu\mathbf{k},\mathbf{q}}$  is the projection of the lattice periodic KS wave functions onto empty states, where  $P^c = (1 - P^v)$  and  $P^v = \sum_{\nu} |\psi_{\nu\mathbf{k}+\mathbf{q}}\rangle \langle\psi_{\nu\mathbf{k}+\mathbf{q}}|$  is the projector onto filled valence states. The first-order expansion of the KS equations gives the Sternheimer equation [60]

$$\left( \hat{H}_{\mathbf{k}+\mathbf{q}}^{KS} - \epsilon_{\nu\mathbf{k}} \right) \partial\psi_{\nu\mathbf{k},\mathbf{q}} = - \left( \partial_{\kappa\alpha\mathbf{q}} v^{KS} - \partial\epsilon_{\nu\mathbf{k}} \right) \psi_{\nu\mathbf{k}}, \quad (22)$$

in which the unperturbed wave functions were written by explicitly indicating the wavevector  $\mathbf{k}$  and band index  $\nu$ , while the perturbed wavefunctions are projected onto the manifold of wave vectors  $\mathbf{k} + \mathbf{q}$ .  $\hat{H}_{\mathbf{k}+\mathbf{q}}^{KS} = e^{-i(\mathbf{k}+\mathbf{q})\cdot\mathbf{r}} \hat{H}^{KS} e^{i(\mathbf{k}+\mathbf{q})\cdot\mathbf{r}}$  where  $\hat{H}^{KS}$  is the unperturbed KS Hamiltonian, Eq. (1), and  $\partial_{\kappa\alpha\mathbf{q}} v^{KS}$  is the first-order variations of the KS potential

$$\partial_{\kappa\alpha\mathbf{q}} v^{KS}(\mathbf{r}) = \partial_{\kappa\alpha\mathbf{q}} V(\mathbf{r}) + e^2 \int \frac{\partial_{\kappa\alpha\mathbf{q}} n(\mathbf{r}')}{|\mathbf{r} - \mathbf{r}'|} e^{-i\mathbf{q}\cdot(\mathbf{r}-\mathbf{r}')} d\mathbf{r}' + \left. \frac{d_{\kappa\alpha\mathbf{q}} V^{xc}}{dn} \right|_{n=n(\mathbf{r})} \partial_{\kappa\alpha\mathbf{q}} n(\mathbf{r}). \quad (23)$$

By expressing  $\partial n$  in terms of a sum over the whole spectrum of the unperturbed Hamiltonian, both occupied and empty states, it becomes evident that contributions to  $\partial n$  coming from only occupied states will vanish [42]. Only perturbations that couple the occupied-state manifold with the empty-state manifold will contribute. At the same time, the right-hand side of Eq. (22) depends only on occupied states, while its left-hand side is ill-conditioned because the possibility of null eigenvalues of the linear operator. In order to make Eq. (22) nonsingular, both sides are projected onto the empty conduction states by the projector  $P^c$ . Additionally, by adding  $P^v P^c \partial\psi_{\nu} = 0$  to the left-hand side of Eq. (22) we remove any null eigenvalues without changing the equation:

$$\left( \hat{H}_{\mathbf{k}+\mathbf{q}}^{KS} + \alpha P_{\mathbf{k}+\mathbf{q}}^v - \epsilon_{\nu\mathbf{k}} \right) \partial\tilde{\psi}_{\nu\mathbf{k},\mathbf{q}} = -(1 - P_{\mathbf{k}+\mathbf{q}}^v) \partial_{\kappa\alpha\mathbf{q}} v^{KS} \psi_{\nu\mathbf{k}}. \quad (24)$$

Within DFPT the responses to perturbations of different wavelengths are decoupled, which allows one to calculate vibrational properties at any wavevector without resorting to large supercells.[59] This is one of the greatest advantages compared to other methods such as frozen-phonon [62, 63] or molecular dynamics methods [64, 65]. In practice, Eqs. (21), (23) and (24) are solved self-consistently, just like the KS equations within DFT. They form a generalized linear problem, since the KS perturbation,  $\partial v^{KS}$ , depends linearly on the

electron-density linear response,  $\partial n$ , which in turn is a linear functional of the variation of the KS wavefunctions,  $\partial\psi$ . In practice, the initial KS perturbation is set to be equal to the external potential, Eq. (13). By solving the Sternheimer equation one obtains the induced electron-density linear response, Eq. (21), which is used to get first-order perturbations of the Hartree and exchange-correlation potentials. Equation (23) then defines a new first-order perturbation of KS potential in the Sternheimer equation. This procedure is repeated until the convergence of  $\partial n$  is reached.

### III. CHARGE AND THERMAL TRANSPORT

The study of the dynamics of electrons and phonons in materials, and particularly, thermoelectric effects, belong to the extremely vast field of non-equilibrium statistical physics. The macroscopic properties of systems that are not in thermodynamic equilibrium are generally described in terms of their microscopic interactions through either kinetic equations, such as the Kadanoff-Baym [66, 67] or Bloch-Boltzmann formalisms [68], or by using linear response theory based on the Kubo equations [69]. Both approaches consider only near-equilibrium situations with linearized irreversible processes, in which the cornerstone property is the fluctuation-dissipation theorem [70]. The relation between the Bloch-Boltzmann formalism and Kubo approach was discussed by Thouless [71], while the derivation of the semiclassical Bloch-Boltzmann formalism from the purely many-body quantum framework of Kadanoff-Baym was given by Poncé et.al. [72]. The double temporal dependence of the nonequilibrium Green's functions within Kadanoff-Baym equations, which stems from memory and coherence effects, makes the computational cost of such calculations very demanding. Only recently have these equations been implemented using first-principles methods within the completed collision approximation.[73] Such developments may eventually overcome the limitations of semiclassical approaches, however currently first-principles calculations are still mainly based on the semiclassical Bloch-Boltzmann formalism using the Boltzmann Transport Equation (BTE).

### A. Justification for the Bloch-Boltzmann formalism

The justification for the applicability of the Bloch-Boltzmann formalism to the dynamics of electrons and phonons in materials rests on the concept of quasiparticles within Landau Fermi liquid theory [74, 75]. Electrons can be considered to be wavepackets that obey Newtonian laws of motion [76]. For a wavepacket with well defined momentum,  $p = \hbar k$ , and hence small uncertainty on the scale of the Fermi momentum,  $\Delta k \ll k_F$ , the uncertainty principle guarantees that  $\Delta x \Delta(\hbar k) \sim \hbar \rightarrow \Delta x \sim \frac{1}{\Delta k} \gg \frac{1}{k_F} \sim a$ , where  $a$  is the lattice constant. Thus, the typical size of the electron wavepacket is much larger than the lattice constant,  $\Delta x \gg a$ . When this picture is valid, the electron distribution function can be defined over phase space cells larger than  $\hbar^3$ , the uncertainty principle is not violated, and the BTE can be justified. It assumes that classical external fields are varying sufficiently slowly in space and time to justify the use of electron wavepackets. This approach enables us to relate the transport properties to the Bloch band structure.

Purely quantum limitations have to be taken into account and the validity condition of the BTE can be related to the Peierls inequality [77] for non-degenerate semiconductors,  $\frac{\hbar}{\tau} \ll k_B T$ . This means that the time interval in which the distribution function evolves should be much smaller than the relaxation time. For metals, this condition can be smoothed by considering  $\frac{\hbar}{\tau(\epsilon_F)} \ll \epsilon_F$  [77], which can be related to the Mott-Ioffe-Regel criterion [78]

$$k_F l \gg 1 , \quad (25)$$

where  $k_F$  is the Fermi wave vector and  $l$  is the mean free path of the carriers. When this criterion is not fulfilled, such as in strongly correlated bad metals [79], the BTE is no longer applicable since the system of interest may not support the existence of long-lived quasiparticles as described by Landau Fermi liquid theory [80]. Also, another subtle assumption that justifies the BTE is the random phase approximation. Within this approximation, the distribution function is only given by diagonal terms of the density matrix, while off-diagonal elements are neglected. Kohn and Luttinger provided a rigorous mathematical formalism to justify that off-diagonal elements are indeed suppressed by considering an ensemble average over a random distribution of impurities.[81, 82]

## B. Boltzmann Transport Equation (BTE)

The Boltzmann Transport Equation describes the propagation of electron or phonon distribution functions,  $f_{n\mathbf{k}}(\mathbf{r}, t)$  or  $N_{\nu\mathbf{q}}(\mathbf{r}, t)$ , respectively. The distribution functions give the probability that an electron (phonon) occupies a state with momentum  $\mathbf{k}$  and band  $n$  (momentum  $\mathbf{q}$  and branch  $\nu$ ) at position  $\mathbf{r}$  and time  $t$ .

In the diffusive transport limit and the presence of a temperature gradient ( $\nabla T$ ) and applied electric ( $\mathbf{E}$ ) and magnetic fields ( $\mathbf{B}$ ), carrier transport properties can be obtained by solving the semiclassical BTE for the nonequilibrium carrier distribution function  $f_{n,\mathbf{k}} = f(\epsilon_{n,\mathbf{k}})$

$$\frac{\partial f_{n,\mathbf{k}}}{\partial t} + \mathbf{v}_{n,\mathbf{k}} \cdot \nabla_{\mathbf{r}} f_{n,\mathbf{k}} - \frac{\mathbf{F}}{\hbar} \cdot \nabla_{\mathbf{k}} f_{n,\mathbf{k}} = \left( \frac{\partial f_{n,\mathbf{k}}}{\partial t} \right)_{\text{coll}}. \quad (26)$$

The electronic band velocity of the carrier in the state  $\{n, \mathbf{k}\}$  with energy  $\epsilon_{n,\mathbf{k}}$  is given by  $\mathbf{v}_{n,\mathbf{k}} = \frac{1}{\hbar} \nabla_{\mathbf{k}} \epsilon_{n,\mathbf{k}}$ , considering the diagonal matrix elements of the velocity operator and ignoring the Berry curvature.[83] The external force is given by  $\mathbf{F} = e(\mathbf{E} + \mathbf{v}_{n,\mathbf{k}} \times \mathbf{B})$ , where  $e$  is the absolute value of the charge of the carriers. In this equation, the temporal evolution of the electron distribution function results from a balance between drift and collision terms. The drift term on the left-hand side of Eq. (26) is an external field-driven flow of the space and momentum variables, while the collision term on the right-hand side accounts for any relevant scattering mechanisms within the diffusive or hydrodynamic regime. An analogous BTE can be written for the phonon distribution function,  $N_{\nu\mathbf{q}}(\mathbf{r}, t)$ , where the phonons follow the Bose-Einstein distribution at equilibrium and are not subject to the external force,  $\mathbf{F}$ . The electronic and phononic scattering mechanisms will be discussed in Sect. III E.

The knowledge of  $f_{n,\mathbf{k}}$  allows for the evaluation of the charge current density,

$$\mathbf{j} = -\frac{2e}{V} \sum_n \sum_k \mathbf{v}_{n,\mathbf{k}} f_{n,\mathbf{k}} = -\frac{2e}{(2\pi)^3} \sum_n \int \mathbf{v}_{n,\mathbf{k}} f_{n,\mathbf{k}} d\mathbf{k}, \quad (27)$$

and the heat energy flux density,

$$\mathbf{j}_Q = \frac{2}{V} \sum_n \sum_{\mathbf{k}} (\epsilon_{n,\mathbf{k}} - \mu) \mathbf{v}_{n,\mathbf{k}} f_{n,\mathbf{k}} = \frac{2}{(2\pi)^3} \sum_n \int (\epsilon_{n,\mathbf{k}} - \mu) \mathbf{v}_{n,\mathbf{k}} f_{n,\mathbf{k}} d\mathbf{k}, \quad (28)$$

where the factor of 2 appears due to the electron spin,  $V$  is the crystal's volume, and  $\mu$  is the chemical potential.

In the next section we discuss the solution of the BTE in the relaxation time approximation for the case of charge carriers; the solution for phonons is analogous. The iterative approach to solving the BTE will be presented in Sect. III F.

### C. Relaxation Time Approximation (RTA)

The collision term on the right-hand side of Eq. (26) drives the system towards a steady state. This scattering term can be expressed by introducing the per-unit-time probability,  $W(n, \mathbf{k}|j, \mathbf{k}')$ , of the transition of the charge carrier from the state  $\{n, \mathbf{k}\}$  to state  $\{j, \mathbf{k}'\}$ , as a result of a particular scattering mechanism. From the principle of detailed balance, the number of charge carriers coming into the state  $\{j, \mathbf{k}'\}$  from  $\{n, \mathbf{k}\}$  is the same as the number coming out from  $\{j, \mathbf{k}'\}$  into  $\{n, \mathbf{k}\}$ . That is, the scattering processes are equally likely going forward or in reverse. This allows us to write

$$\left( \frac{\partial f_{n,\mathbf{k}}}{\partial t} \right)_{coll} = \sum_{j,\mathbf{k}'} [W(j, \mathbf{k}'|n, \mathbf{k}) f_{j,\mathbf{k}'} (1 - f_{n,\mathbf{k}}) - W(n, \mathbf{k}|j, \mathbf{k}') f_{n,\mathbf{k}} (1 - f_{j,\mathbf{k}'})] . \quad (29)$$

This condition is a consequence of time-reversal symmetry of the microscopic equations of motion and is sufficient to ensure a positive local entropy production rate for systems out of equilibrium. It is described via the H-theorem[84] by writing the results as a function of H, the negative of the entropy.[85, 86] The intricate dependency of  $f_{n,\mathbf{k}}$  on the linear response distribution function of all other states,  $f_{j,\mathbf{k}'}$ , complicates the solution of the BTE and thus various forms of the RTA are usually applied. Poncé et.al. [72] reviewed different levels of approximations such as the momentum relaxation time approximation (MRTA), the self-energy relaxation time approximation (SERTA)[87], the lowest-order variational approximation (LOVA)[88], and the Ziman resistivity formula for metals.[89]. In general, the computational cost and the accuracy decreases from the former to the latter. Here we focus on the SERTA, which neglects backward scattering rates.[72]

Assuming that the system is close enough to local equilibrium, the non equilibrium distribution function,  $f_{n,\mathbf{k}}$ , differs only slightly from that of the equilibrium state,  $f_{n,\mathbf{k}}^{(0)}$ ; namely  $\Delta f(n, \mathbf{k}) = |f_{n,\mathbf{k}} - f_{n,\mathbf{k}}^{(0)}| \ll f_{n,\mathbf{k}}^{(0)}$ . Consequently,  $f_{n,\mathbf{k}}$  can be expanded to first order as

$$f_{n,\mathbf{k}} = f_{n,\mathbf{k}}^{(0)} - \tau_{n,\mathbf{k}} \mathbf{v}_{n,\mathbf{k}} \cdot \Phi_0(\epsilon) \left( \frac{\partial f^{(0)}}{\partial \epsilon} \right) , \quad (30)$$

where  $\Phi_0(\epsilon) = -e\epsilon - \frac{\epsilon - \mu}{T} \nabla T$  is the generalized disturbing force (dynamic and static) causing the deviation from the equilibrium distribution, and  $\epsilon = \mathbf{E} + (1/e)\nabla\mu = -\nabla(\phi_0 - (\mu/e))$  is the gradient of the electrochemical potential. Using this approximation, Eq. (29) can be written in the RTA as

$$\left( \frac{\partial f_{n,\mathbf{k}}}{\partial t} \right)_{coll} = -\frac{\Delta f(n, \mathbf{k})}{\tau_{n,\mathbf{k}}} , \quad (31)$$

where

$$\frac{1}{\tau_{n,\mathbf{k}}} = \sum_{\mathbf{k}'} \sum_j W(n, \mathbf{k}|j, \mathbf{k}') \left( \frac{1 - f_{j,\mathbf{k}'}^{(0)}}{1 - f_{n,\mathbf{k}}^{(0)}} - \frac{f_{n,\mathbf{k}}^{(0)}}{f_{j,\mathbf{k}'}^{(0)}} \frac{\Delta f(j, \mathbf{k}')}{\Delta f(n, \mathbf{k})} \right), \quad (32)$$

considering both the absence of quantization effects and that  $W(n, \mathbf{k}|j, \mathbf{k}')$  does not depend on  $\mathbf{E}$ ,  $\mathbf{B}$ , or  $\nabla T$ . Substituting Eq. (30) into Eq. (32) we obtain

$$\frac{1}{\tau_{n,\mathbf{k}}} = \sum_{\mathbf{k}'} \sum_j W(n, \mathbf{k}|j, \mathbf{k}') \frac{1 - f^{(0)}(\epsilon')}{1 - f^{(0)}(\epsilon)} \left( 1 - \frac{\tau_{j,\mathbf{k}'} \mathbf{v}_{j,\mathbf{k}'} \cdot \Phi_0(\epsilon')}{\tau_{n,\mathbf{k}} \mathbf{v}_{n,\mathbf{k}} \cdot \Phi_0(\epsilon)} \right). \quad (33)$$

Thus, in the steady-state limit of a homogeneous system with no magnetic field, Eq. (26) simplifies to

$$\mathbf{v}_{n,\mathbf{k}} \cdot \nabla_{\mathbf{r}} f_{n,\mathbf{k}} - \frac{e\mathbf{E}}{\hbar} \cdot \nabla_{\mathbf{k}} f_{n,\mathbf{k}} = -\frac{\Delta f(n, \mathbf{k})}{\tau_{n,\mathbf{k}}}, \quad (34)$$

from which the non equilibrium distribution function is obtained provided that  $\tau_{n,\mathbf{k}}$  does not depend on  $\mathbf{E}$  or  $\nabla T$ .

A common additional approximation is the assumption that  $W(n, \mathbf{k}|j, \mathbf{k}')$  does not depend on  $\mathbf{k}$  and  $\mathbf{k}'$  separately, but only on their magnitudes and the angle between them,  $W(n, \mathbf{k}|j, \mathbf{k}') = W_{n,j}(|\mathbf{k}|, |\mathbf{k}'|, \mathbf{k} \cdot \mathbf{k}')$ . Then, Eq. (33) may be rewritten as [90]

$$\frac{1}{\tau_{n,k}} = \sum_{\mathbf{k}'} \sum_j W(n, \mathbf{k}|j, \mathbf{k}') \left( 1 - \frac{\mathbf{k} \cdot \mathbf{k}'}{k^2} \right), \quad (35)$$

assuming that charge carrier scattering is purely elastic and the dispersion relation is an arbitrary spherically symmetric function of the magnitude of the wavevector (not necessarily parabolic), so that  $\epsilon(|\mathbf{k}|) = \epsilon(|\mathbf{k}'|)$ . Although Eq. (35) was derived for isotropic bands, results obtained from it have been used to study transport properties of chalcogenides, which are anisotropic [91–93]. This is possible because the transport properties along the different directions in these materials are mutually independent, except for the magnetoresistance, which critically depends on the anisotropy.

#### D. Thermoelectric kinetic coefficients tensors

The tensorial formalism based on the Onsager-de Groot-Callen model[94–98] is appropriate to discuss thermoelectric (TE) effects for anisotropic materials using the thermodynamics of irreversible processes and linear response theory. In this model, the flux of charge carriers and thermal energy is described in terms of a kinetic matrix and generalized forces. (For

reviews see Goupil [99] and Feldhoff.[100]) In summary, the off-diagonal coupling between the electronic current density,  $\mathbf{j}$ , and heat energy flux density,  $\mathbf{j}_Q$ , can be written:

$$\begin{bmatrix} \mathbf{j} \\ \mathbf{j}_Q \end{bmatrix} = \begin{bmatrix} \mathbf{L}^{11} & \mathbf{L}^{12} \\ \mathbf{L}^{21} & \mathbf{L}^{22} \end{bmatrix} \cdot \begin{bmatrix} \varepsilon \\ -\frac{\nabla T}{T} \end{bmatrix} \quad (36)$$

in which,  $\mathbf{L}^{11}$ ,  $\mathbf{L}^{12}$ ,  $\mathbf{L}^{21}$ ,  $\mathbf{L}^{22}$  are the moments of the generalized transport coefficients. The Onsager reciprocity relations guarantee  $\mathbf{L}^{12} = \mathbf{L}^{21}$  [94, 95, 98]. These kinetic coefficients are defined by

$$\Lambda^{(\alpha)}(\mu; T) = e^2 \int \Xi(\epsilon, \mu, T)(\epsilon - \mu)^\alpha \left( -\frac{\partial f^{(0)}(\mu; \epsilon, T)}{\partial \epsilon} \right) d\epsilon, \quad (37)$$

with  $\mathbf{L}^{11} = \Lambda^{(0)}$ ,  $\mathbf{L}^{21} = \mathbf{L}^{12} = -(1/e)\Lambda^{(1)}$ , and  $\mathbf{L}^{22} = (1/e^2)\Lambda^{(2)}$ , in which  $\Xi(\epsilon, \mu, T)$  is the transport distribution kernel (TDK) given by

$$\Xi(\epsilon, \mu, T) = \int \sum_n \mathbf{v}_{n,\mathbf{k}} \otimes \mathbf{v}_{n,\mathbf{k}} \tau_{n,k}(\mu, T) \delta(\epsilon - \epsilon_{n,\mathbf{k}}) \frac{d\mathbf{k}}{8\pi^3}. \quad (38)$$

In the dynamic steady state, thermoelectric properties can be obtained by considering specific experimental conditions. For an isothermal situation ( $\nabla T = 0$ ), the charge current,  $\mathbf{j}$ , obeys Ohm's law and the kinetic coefficient tensor can be identified with the electrical conductivity tensor,  $\sigma = \Lambda^{(0)}$ . As pointed out by Feldhoff [100], even with the isothermal condition,  $\mathbf{j}$  is accompanied by an entropy current whose magnitude and direction depend on the Seebeck coefficient,  $S$ , which can be viewed as a quantity that measures entropy flow per unit charge.  $S$  is obtained by requiring the electric current to vanish, so the electrochemical potential gradient and the thermal gradient are balanced. Then  $S$  is given by the ratio between them,  $S = (eT)^{-1}\Lambda^{(1)}/\Lambda^{(0)}$ .

As one of the most sensitive probes of the carriers in a material, the Seebeck measurement is related to the heat per carrier over temperature or the entropy per carrier, as pointed out earlier. It suggests that  $S$  can provide information about *i*) the sign of the charge of the carriers and *ii*) the characteristic energy associated with the carriers. However, the former result does not hold in a few cases, such as noble metals, where  $S$  and the Hall coefficient have diverging signs.[101] This has been attributed to the complex energy dependence of the mean free path due to the electron-phonon scattering.[102]. The second result generally holds and can be used, for example, to distinguish metals and semiconductors by comparing the magnitude and temperature behavior of  $S$ . While metals exhibit values of  $S$  that decrease

with temperature and have magnitudes much smaller than  $k_B/e \approx 87\mu V/K$ , semiconductors present much larger magnitudes that increase with temperature.[101]

The zero electric current condition yields Fourier's law, in which the charge carrier contribution to the thermal conductivity tensor is given by

$$\kappa_{el} = (e^2 T)^{-1} \left( \Lambda^{(1)} \cdot \Lambda^{(0)^{-1}} \cdot \Lambda^{(1)} - \Lambda^{(2)} \right) . \quad (39)$$

The second term within brackets corresponds to the thermal conductivity due to the carrier transport under isoelectrochemical conditions, while the first term is the power factor ( $PF = \sigma S^2$ ) related to the thermal conductivity that couples to the charge current. This is responsible for thermoelectric conversion, that is, the transfer of energy from an entropy current to an electric current or vice versa.[100, 103]

### E. Scattering mechanisms within semiclassical BTE

In order to solve the BTE for either charge carriers or phonons we need to provide the collision term on the right-hand side of Eq. (26). This term incorporates the various microscopic scattering mechanisms that are detailed below.

#### 1. *Electron-phonon interaction*

The electron-phonon interaction is a key factor in determining functional properties of materials such as thermoelectric transport properties. The electron-phonon coupling hamiltonian can be derived within DFT by expanding the KS Hamiltonian to first-order in  $\Delta\xi_{\kappa p}$ , the displacements of the nuclei from their equilibrium positions,  $\xi_{\kappa p}^0$ :

$$V^{KS}(\{\xi_{\kappa p}\}) = V^{KS}(\{\xi_{\kappa p}^0\}) + \sum_{\kappa\alpha p} \frac{\partial V^{KS}}{\partial \xi_{\kappa\alpha p}} \Delta\xi_{\kappa\alpha p} . \quad (40)$$

Extending the expansion to second-order results in Debye-Waller terms [104] that will not be discussed in the present review, since these terms are purely real and do not affect el-ph relaxation times. [105] The operator for the phonon perturbation potential is given in terms of quantized normal mode coordinates using phonon annihilation and creation operators ( $b_{\nu\mathbf{q}}, b_{\nu\mathbf{q}}^\dagger$ ):

$$V^{KS} = V^{KS}(\{\xi_{\kappa p}^0\}) + \frac{1}{N_p^{1/2}} \sum_{\nu\mathbf{q}} \Delta_{\nu\mathbf{q}} V^{KS}(\hat{b}_{\nu\mathbf{q}} + \hat{b}_{-\nu\mathbf{q}}^\dagger) , \quad (41)$$

where

$$\Delta_{\nu\mathbf{q}}V^{KS} = e^{i\mathbf{q}\cdot\mathbf{r}}\Delta_{\nu\mathbf{q}}v^{KS}, \quad (42)$$

and

$$\Delta_{\nu\mathbf{q}}v^{KS} = c_{\nu\mathbf{q}} \sum_{\kappa\alpha p} \left( \frac{M_0}{M_\kappa} \right)^{\frac{1}{2}} e_{\kappa\alpha,\nu}(\mathbf{q}) e^{-i\mathbf{q}\cdot(\mathbf{r}-\mathbf{R}_p)} \frac{\partial V^{KS}}{\partial \xi_{\kappa\alpha}} \Big|_{\mathbf{r}=\mathbf{R}_p}, \quad (43)$$

with  $c_{\nu\mathbf{q}}$  being the zero-point displacement amplitude. Using the electron annihilation and creation operators,  $(a_{n\mathbf{k}}, a_{n\mathbf{k}}^\dagger)$ , the first-principles el-ph perturbation Hamiltonian is

$$\begin{aligned} \hat{H}^{el-ph} &= \sum_{n\mathbf{k}, n'\mathbf{k}'} \langle \phi_{n'\mathbf{k}'} | V^{KS}(\{\xi_{\kappa p}\}) - V^{KS}(\{\xi_{\kappa p}^0\}) | \phi_{n\mathbf{k}} \rangle \hat{b}_{\nu\mathbf{q}} \hat{a}_{n\mathbf{k}}^\dagger \hat{a}_{n'\mathbf{k}'} \\ &= \frac{1}{N_p^{1/2}} \sum_{\mathbf{k}, \mathbf{q} m n \nu} g_{m n \nu}(\mathbf{k}, \mathbf{q}) \hat{a}_{n\mathbf{k}}^\dagger \hat{a}_{n'\mathbf{k}'} (\hat{b}_{\nu\mathbf{q}} + \hat{b}_{-\nu\mathbf{q}}^\dagger), \end{aligned} \quad (44)$$

where the electron-phonon matrix element has been defined as

$$g_{m n \nu}(\mathbf{k}, \mathbf{q}) = \langle u_{m\mathbf{k}+\mathbf{q}} | \Delta_{\nu\mathbf{q}}v^{KS} | u_{n\mathbf{k}} \rangle, \quad (45)$$

which can be computed by DFPT (see Sect. II C), using Eq. (21) [106]. From the electron-phonon Hamiltonian, the el-ph relaxation times (RT) can be derived in different ways, such as perturbatively via Feynman-Dyson diagram techniques [107, 108] or nonperturbatively via Hedin-Baym equations within quantum field theory [106, 109, 110]. Also, within the Born approximation, the RT can be derived by considering all scatterings in which an electron emits or absorbs one phonon via Fermi's golden rule, along with the rate equation for the time-dependent electron distribution functions [111]. The latter approach was derived in Section III F. In all cases the RT is given by the imaginary part of the electron self energy,  $\Sigma$ :

$$\begin{aligned} \text{Im} [\Sigma_{n,\mathbf{k}}(\epsilon, T)] &= \pi \sum_{m,\nu} \int_{BZ} \frac{d\mathbf{q}}{\Omega_{BZ}} |g_{m n \nu}(\mathbf{k}, \mathbf{q})|^2 \\ &\times \left[ [n_{\mathbf{q}\nu}(T) + f_{m\mathbf{k}+\mathbf{q}}] \delta(\epsilon - (\epsilon_{m\mathbf{k}+\mathbf{q}} - \epsilon_F) + \omega_{\mathbf{q}\nu}) \right. \\ &\left. + [n_{\mathbf{q}\nu}(T) + 1 - f_{m\mathbf{k}+\mathbf{q}}] \delta(\epsilon - (\epsilon_{m\mathbf{k}+\mathbf{q}} - \epsilon_F) - \omega_{\mathbf{q}\nu}) \right], \end{aligned} \quad (46)$$

where  $g_{m n \nu}(\mathbf{k}, \mathbf{q})$  are the el-ph matrix elements,  $\Omega_{BZ}$  is the volume of the Brillouin zone (BZ) and the Dirac  $\delta$ -functions enforce energy conservation for emission or absorption of a phonon with wavevector  $\mathbf{q}$  and mode  $\nu$  and energy  $\hbar\omega_{\mathbf{q}\nu}$ . Equation (46) contains the

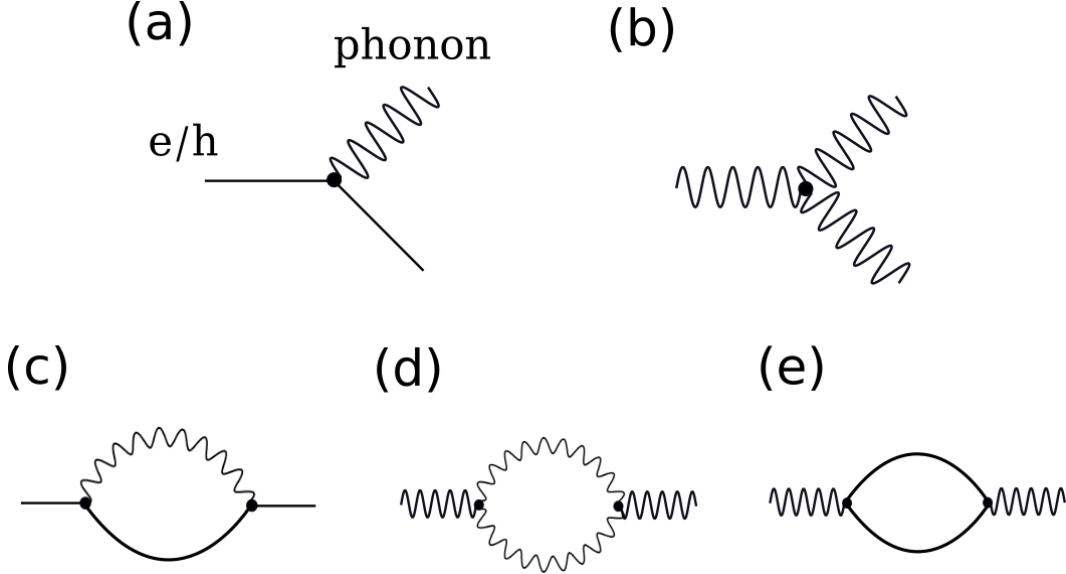


FIG. 2. Feynman diagrams showing (a) electron-phonon and (b) three-phonon interactions, as well as the self-energy diagrams representing (c) electron-phonon, (d) phonon-phonon, and (e) phonon-electron scattering.

dynamical structure of the electron-phonon interaction on the scale of the phonon energy. The temperature dependence comes from the electron and phonon distribution functions. Eq. (46) corresponds to the imaginary part of the lowest-order Feynman diagram (*GD* self-energy) shown in Fig. 2(c). Migdal theory demonstrated that non-adiabatic terms are less important in higher order diagrams, justifying the truncation at the lowest order diagram [112, 113].

Since the RTs are resolved for different bands and  $\mathbf{k}$ -points, after integrating over all phonon modes and  $\mathbf{q}$ -points, first-principles calculations can provide rich microscopic information. In order to converge the el-ph RTs when calculating transport properties, very dense  $\mathbf{k}$  and  $\mathbf{q}$  meshes are needed [114, 115], so interpolation schemes have to be used instead of brute-force DFPT calculations. In Sect. IV A we discuss interpolation schemes developed for this aim.

## 2. Frölich dipole and quadrupolar el-ph coupling

While screening lengths are very short in metals, long-range (LR) el-ph interactions may appear in semiconductors and insulators due to the incomplete screening of the potential

generated by the atomic displacements. In particular, polar materials, with two or more atoms in the unit cell, exhibit nonzero Born effective charge tensors [116, 117]. In these systems, the most relevant contribution to the perturbation potential ( $\partial V^{KS}/\partial \xi_{\kappa\alpha}$ ) is a dipole decaying as  $|\mathbf{R}_p^{-2}|$ , and thus long-range el-ph interactions occur in the long-wavelength limit ( $\mathbf{q} \rightarrow 0$ ), and are responsible for the longitudinal optical-transverse optical (LO-TO) splitting of the optical frequencies [118] and the divergence of the el-ph matrix elements, known as Fröhlich coupling [119]. This polar scattering was first discussed by Fröhlich [119], Callen [120], and Howarth and Sondheimer [121].

In polar materials lacking inversion symmetry the piezoelectric (PE) el-ph interaction plays an important role, in addition to the dipolar and deformation-potential contributions. Such interactions come from the strain induced by acoustic phonons and can be expressed as a function of the macroscopic piezoelectric constants of the material [68]. In a more general approach, all these el-ph interactions, including dipolar, deformation-potential and piezoelectric contributions, can be expressed as a multipole Vogl expansion of the el-ph potential [122, 123]. The divergent Fröhlich el-ph interaction comes from the dipole term, while the piezoelectric interaction comes from both the dipole and the quadrupole terms [122]. Even though the Fröhlich coupling is dominant for LO modes [117], quadrupolar interactions can dominate for the TO and acoustic modes [122].

Because Wannier-Fourier (WF) interpolation (described in Sect. IV A) is based on the spatial localization of the el-ph coupling, first-principles treatment of the LR interaction is not amenable to WF interpolation, since it requires a very large number of e-p matrix elements to attain convergence [124]. Verdi [117] and Sjakste et al. [125] developed a first-principles approach to adapt the WF interpolation to the case of dipole Fröhlich coupling in polar materials, and the importance of the next-to-leading order term in the Vogl expansion beyond the dipolar contribution was addressed by Brunin [126], Jhalani [127] and Park [128]. In summary, those works separate the LR dipole and quadrupole contributions to the el-ph matrix elements from the short-range (SR) part:

$$g_{mn\nu}(\mathbf{k}, \mathbf{q}) = g_{mn\nu}^L(\mathbf{k}, \mathbf{q}) + g_{mn\nu}^S(\mathbf{k}, \mathbf{q}) \quad (47)$$

$$= g_{mn\nu}^D(\mathbf{k}, \mathbf{q}) + g_{mn\nu}^Q(\mathbf{k}, \mathbf{q}) + g_{mn\nu}^S(\mathbf{k}, \mathbf{q}) , \quad (48)$$

where  $g_{mn\nu}^D(\mathbf{k}, \mathbf{q})$  is the first-principles Fröhlich el-ph matrix element, written in terms of

Born effective charges [117].

$$\begin{aligned}
g_{mn,\nu}^D(\mathbf{k}, \mathbf{q}) = & i \frac{e^2}{\Omega_{uc}\epsilon_0} \sum_{\kappa} \left( \frac{\hbar}{2N_p M_{\kappa} \omega_{\mathbf{q}\nu}} \right)^{\frac{1}{2}} \\
& \times \sum_{\mathbf{G} \neq -\mathbf{q}} \frac{(\mathbf{q} + \mathbf{G}) \cdot \mathbf{Z}_{\kappa}^* \cdot \mathbf{e}_{\kappa\nu}(\mathbf{q})}{(\mathbf{q} + \mathbf{G}) \cdot \zeta_{\infty} \cdot (\mathbf{q} + \mathbf{G})} \\
& \times \langle \Psi_{m\mathbf{k}+\mathbf{q}} | e^{i(\mathbf{k}+\mathbf{q}) \cdot \mathbf{r}} | \Psi_{n\mathbf{k}} \rangle , \quad (49)
\end{aligned}$$

in which  $N_p$  is the number of unit cells in the Born-von Kármán supercell,  $\Omega_{uc}$  is the volume of the unit cell,  $\mathbf{G}$  is a reciprocal lattice vector,  $\mathbf{Z}^* = Z_{\alpha,\beta}^*$  is the Born effective charge tensor,  $\mathbf{e}_{\kappa\nu}(\mathbf{q})$  is a phonon eigenmode normalized within the unit cell,  $\zeta_{\infty} = \zeta_{\alpha,\beta}^{\infty}$  corresponds to the high-frequency dielectric constant tensor,  $\epsilon_0$  is the vacuum permittivity, and  $\hbar$  is the reduced Planck constant.  $\langle \Psi_{m\mathbf{k}+\mathbf{q}} | e^{i(\mathbf{k}+\mathbf{q}) \cdot \mathbf{r}} | \Psi_{n\mathbf{k}} \rangle = [U^{\mathbf{k}+\mathbf{q}} U^{\mathbf{k}\dagger}]_{mn}$  are phase factors given in terms of rotation matrices,  $U^{\mathbf{k}+\mathbf{q}}$ , that appear in the definition of the maximally localized Wannier functions (MLWFs), Eq. (6)[30].

The quadrupole el-ph matrix elements imply summations over the Cartesian indices  $\alpha$ ,  $\beta$  and  $\gamma$  and can be expressed as [127, 128]

$$\begin{aligned}
g_{mn,\nu}^Q(\mathbf{k}, \mathbf{q}) = & \frac{e^2}{\Omega_{uc}\epsilon_0} \sum_{\kappa} \left( \frac{\hbar}{2M_{\kappa} \omega_{\mathbf{q}\nu}} \right)^{\frac{1}{2}} \\
& \times \sum_{\mathbf{G} \neq -\mathbf{q}} \frac{\frac{1}{2}(q_{\alpha} + G_{\alpha})(Q_{\kappa,\beta}^{\alpha\gamma} \mathbf{e}_{\kappa\nu}^{(\beta)}(\mathbf{q}))(q_{\gamma} + G_{\gamma})}{(q_{\alpha} + G_{\alpha})\zeta_{\alpha\gamma}(q_{\gamma} + G_{\gamma})} \\
& \times \langle \Psi_{m\mathbf{k}+\mathbf{q}} | e^{i(\mathbf{q}+\mathbf{G}) \cdot (\mathbf{r}-\xi_{\kappa})} | \Psi_{n\mathbf{k}} \rangle , \quad (50)
\end{aligned}$$

where  $Q_{\kappa,\beta}^{\alpha\gamma}$  are the dynamical quadrupoles that correspond to the second order term of a multipole expansion of the charge density induced by an atomic displacement in the long-wavelength limit, that can also be calculated using the DFPT approach [47–49, 129]. As shown for GaN and PbTiO<sub>3</sub> [127, 128], the inclusion of dipole and quadrupole interactions corrects the long-range el-ph coupling in these polar materials. Also, the application of this approach to Si has demonstrated that quadrupole interactions develop an important role even for nonpolar materials [128].

### 3. Screening for long-range interactions

The above expressions represent a first-principles generalization of the Fröhlich and quadrupolar el-ph coupling. However, this theory is limited to undoped systems, neglecting screening effects due to the presence of free carriers. The effect of this additional screening is related to the variation of the dielectric properties in the long-wavelength limit and it was discussed recently by Ren et al. [130] on the basis of the semi-empirical Thomas-Fermi formalism applied to doped half-Heusler semiconductors. Also, on the basis of a linear-response and dielectric matrix formulation [38, 47, 122], Macheda et al. [131] developed a first-principles framework to take into account the screening effects due to the presence of free carriers in doped semiconductors at finite temperature. In general, free carriers screen out the electric field, resulting in both a weakening of the LR e-p coupling as more carriers are added to the system, and a shift of the frequency of the LO mode [132] leading into a reduction of the LO-TO splitting. Neglecting screening effects clearly yields an overestimation of LR el-ph relaxation times and mobility.

A quantification of those effects was addressed within a quasi-static approximation by Ehrenreich [132], in which the LR el-ph matrix element is weakened by a factor of  $1 - (r_\infty \mathbf{q})^{-2}$ , where  $r_\infty$  is the screening radius,

$$r_\infty^{-2}(n, \mathbf{k}) = \frac{4\pi e^2}{\zeta_\infty} \int \left( -\frac{\partial f_\mu(T, \epsilon)}{\partial \epsilon_{n, \mathbf{k}}} \right) g(\epsilon) d\epsilon, \quad (51)$$

and  $g(\epsilon)$  is the density of states (DOS),

$$g(\epsilon) = \int \sum_n \delta(\epsilon - \epsilon_{n, \mathbf{k}}) \frac{d\mathbf{k}}{8\pi^3} = \frac{1}{\Omega_{BZ} N_{\mathbf{k}}} \sum_{n, \mathbf{k}} \frac{\delta(\epsilon - \epsilon_{n, \mathbf{k}})}{d\epsilon}. \quad (52)$$

The eigenfrequency shift of the LO phonons reads

$$(\omega^{LO})^2 = (\omega^{TO})^2 \left( \frac{\zeta_0/\zeta_\infty + (r_\infty \mathbf{q})^{-2}}{1 + (r_\infty \mathbf{q})^{-2}} \right), \quad (53)$$

where  $\omega^{TO}$  is the TO mode eigenfrequency. The eigenfrequency of the LO vibration is strongly reduced, further altering the e-p matrix elements [93]. The resulting change in the LR RT is given by the following band-dependent factor:

$$F_{\text{pol}}(n, \mathbf{k}) = \left[ 1 - \frac{1}{2(r_\infty(n, \mathbf{k}) \cdot \mathbf{k})^2} \times \ln[1 + 4(r_\infty(n, \mathbf{k}) \cdot \mathbf{k})^2] + \frac{1}{1 + 4(r_\infty(n, \mathbf{k}) \cdot \mathbf{k})^2} \right]^{-1}. \quad (54)$$

By combining Eqs. (46), (49), and (54), we arrive at expressions for the RT corresponding to both non-polar ( $\tau_{\text{npol}}$ ) and screened polar ( $\tau_{\text{pol}}$ ) phonon scattering. The non-polar e-p RT is given by

$$\frac{1}{\tau_{\text{npol}}(n, \mathbf{k})} = 2 \text{Im} \Sigma_{n, \mathbf{k}}[\epsilon = 0, T, g_{mn, \theta}^S(\mathbf{k}, \mathbf{q})], \quad (55)$$

and the screened polar e-p RT reads

$$\frac{1}{\tau_{\text{pol}}(n, \mathbf{k})} = 2 \text{Im} \Sigma_{n, \mathbf{k}}[\epsilon = 0, T, g_{mn, \theta}^L(\mathbf{k}, \mathbf{q})] \times F_{\text{pol}}(n, \mathbf{k}). \quad (56)$$

It is important to note that dynamical features of the screening were neglected here, since their effect is regarded to be quite small [93]. Also, the energy dependence of the RT is also changed because of the energy dependence of the screening that enters through  $r_\infty$ . This quasi-static approach has been applied recently to address the screened Fröhlich coupling in thermoelectric layered materials [133, 134] and will be reviewed later in this article.

#### 4. Defect scattering

Carrier scattering by defects is the dominant scattering mechanism that limits charge and spin transport in non-degenerate semiconductors at low temperature [135, 136]. In this regime subtle quantum transport effects can be induced by defects.[137–139] Even at higher temperatures, carrier dynamics and thermoelectric properties in highly doped materials can be limited by electron-defect (e-d) scattering. A prominent example is SnSe, in which there is temperature-induced Sn vacancy formation above 600 K [133, 140]. As defects are systematically employed to engineer advanced functional materials and devices [141, 142], in particular, thermoelectric materials [143], the microscopic understanding of e-d scattering from first-principles calculations provides a basis to explore charge and spin dynamics in materials in the presence of neutral and ionized defects.

Calculations of e-d scattering have mostly relied on semiempirical models. In particular, ionized defect scattering has been treated theoretically by Brooks and Herring (B-H) [144, 145]. They used a screened Coulomb potential within the Born approximation for the evaluation of transition probabilities due to the scattering of carriers by dilute concentrations randomly distributed, ionized scattering centers. The dilute regime allows one to neglect the perturbations to the electron energy levels as well as complex effects such as the contributions from coherent scattering off pairs of defect centers, which requires a quantum transport

theory [146]. The per-unit-time transition probability for the scattering of charge carriers by ionized defects can be written in the plane-wave approximation as

$$W(\mathbf{k}|\mathbf{k}') = \frac{2\pi}{\hbar} \frac{N_i}{V} \left| \int U(\mathbf{r}) \exp[i(\mathbf{k} - \mathbf{k}') \cdot \mathbf{r}] d\mathbf{r} \right|^2 \delta(\epsilon_{\mathbf{k}'} - \epsilon_{\mathbf{k}}) , \quad (57)$$

where  $U(\mathbf{r})$  is the scattering potential and  $N_i$  is the number of ionized defects. The straightforward application of the long-range Coulomb field,  $U(\mathbf{r}) = e\phi(\mathbf{r}) = \pm e^2/\zeta_0 r$ , with electrostatic potential  $\phi$  due to the presence of positive (donor) or negative (acceptor) defect ions, leads into a logarithmic divergence. Hence a screened Coulomb potential such as

$$U(\mathbf{r}) = \pm \frac{e^2}{\zeta_0 r} (e^{-r/r_0}) , \quad (58)$$

must be considered, where  $r_0$  is the screening radius of the defect ion defined by

$$r_0^{-2}(k) = \frac{4\pi e^2}{\zeta_0} \int -\frac{\partial f^{(0)}(\epsilon)}{\partial \epsilon_k} g(\epsilon) d\epsilon . \quad (59)$$

From Eq. (57) and Fermi's golden rule, the RT for the scattering of charge carriers by ionized defects can be expressed as [91]

$$\tau_{\text{imp}}(k) = \frac{\hbar \zeta_0^2}{2\pi e^4 N_i F_{\text{imp}}(k)} k^2 \left| \frac{\partial \epsilon_k}{\partial k} \right| \quad (60)$$

where

$$F_{\text{imp}}(k) = \ln(1 + \eta) - \frac{\eta}{1 + \eta} , \quad (61)$$

is the screening function, with  $\eta = (2kr_0)^2$ .

More intricate *ab initio* calculations based on the multiple scattering Korringa-Kohn-Rostoker (KKR) Green's function method have also been commonly employed [147–150], even though this method is much more computationally expensive. In general, those calculations start with DFT, in which the Green's functions of a crystal host with a single defect are exactly embedded in the unperturbed crystal host using a Dyson equation. On the other hand, first-principles calculations of e–d scattering on the basis of plane-wave DFT using pseudopotentials or projector augmented waves [151, 152] have faced computational challenges due to the high costs of the supercell approach to determine e–d interaction matrix elements within a perturbative approach. One recently developed method, based only on the primitive cell and Wannier-Fourier interpolation, significantly reduces the computational cost [153, 154]. However, this method was developed only for neutral defects. Since the concentration of ionized defects is usually considerably larger than that of neutral imperfections,[91] an extension of this method to include ionized defects would be necessary.

## 5. Phonon-phonon scattering

Phonon properties can be determined perturbatively by expanding the ionic potential energy in a Taylor series in atomic displacements, as discussed in Sect. II C. The first-derivative term vanishes for a crystal in equilibrium. The second derivative term gives rise to the 2nd-order force constants which describe the phonon band structure through the dynamical matrix in the “harmonic approximation”, Eq. (18). The third derivative term,

$$\frac{\partial^3 E(\mathbf{R})}{\partial \mathbf{R}_I \partial \mathbf{R}_J \partial \mathbf{R}_K}, \quad (62)$$

represents the coupling of three phonons, Fig. 2(b), and is the first to allow for scattering between phonons. Diagrammatically, the phonon-phonon scattering rate is related to the imaginary part of the phonon self-energy contributed by a virtual phonon-phonon pair, as shown in Fig. 2(d). The three-phonon coupling gives contributions to the phonon scattering matrix arising from phonon absorption (two phonons merge into one) and decay (one phonon splits into two). Detailed expressions are given in Ref. 155.

## 6. Phonon-electron scattering

The same electron-phonon coupling that leads to scattering of electrons by phonons can also contribute to scattering of phonons by electrons. The phonon-electron scattering rate is determined by the imaginary part of the phonon self-energy diagram that contains a virtual electron-hole pair, shown in Fig. 2(e). These contributions are often assumed to be smaller than the phonon-phonon scattering, but they have been shown to make a significant contribution in some metals or highly doped semiconductors [156].

## 7. Isotope and boundary scattering of phonons

Two other phonon scattering processes, which might be relevant for specific situations, can be easily incorporated in the phonon scattering matrix. Scattering due to mass disorder, sometimes called isotope scattering, is treated as scattering from an appropriately averaged point defect [157]. The coupling strength is an input, based either on natural isotopic abundance or chosen to match a particular doping scheme. Boundary scattering due to the

physical size of a crystal can be incorporated by a simple term that depends only on the size, the phonon group velocity, and the equilibrium populations. Details are given in Ref. 155.

### 8. Combining scattering processes through Mathiessen's rule

Within the RTA, if there are several scattering mechanisms that are approximately independent, their respective scattering times can be combined using Mathiessen's rule. For example, for charge carriers subject to non-polar and polar phonon scattering, as well as scattering from charged impurities, the total scattering rate that appears in the BTE, Eq. (31) or (34), will be:

$$\frac{1}{\tau_{\text{tot}}} = \frac{1}{\tau_{\text{npol}}} + \frac{1}{\tau_{\text{pol}}} + \frac{1}{\tau_{\text{imp}}} . \quad (63)$$

The temperature dependence of the RT is given indirectly through the phonon and electron distributions within Eq. (46). Additionally, for  $\tau_{\text{pol}}$  and  $\tau_{\text{imp}}$ ,  $T$  and  $\mu$  dependence enters implicitly through their respective screening radii ( $r_\infty$  and  $r_0$ ) as defined in Eq. (51). This dependence on  $\mu$  allows for the study of doped materials, which are important for the optimization of  $zT$  for thermoelectric applications.

## F. Iterative approach for solving the BTE

In some cases it is possible to go beyond the RTA approach to the BTE by using an iterative solution method. From perturbation theory, if the interaction potential is weak enough, the scattering can be treated in the Born approximation and Fermi's golden rule can be used to determine the transition probability of the electronic scattering process  $\{|n\mathbf{k}\rangle\} \rightarrow \{|m\mathbf{k} + \mathbf{q}\rangle\}$ , describing absorption of a phonon with mode  $\{\nu\}$  and wave vector  $\mathbf{q}$ :

$$W_{n\mathbf{k},\nu\mathbf{q}}^{m\mathbf{k}+\mathbf{q}} = \frac{2\pi}{\hbar} |g_{n\mathbf{k},\nu\mathbf{q}}^{m\mathbf{k}+\mathbf{q}}|^2 \delta(\epsilon_{n\mathbf{k}} + \hbar\omega_{\nu\mathbf{q}} - \epsilon_{m\mathbf{k}+\mathbf{q}}) . \quad (64)$$

The transition probability exhibits the microreversibility property which stems from the time-reversal invariance of the microscopic equations of motion. Thus the last equation is equal to the reverse transition  $W_{m\mathbf{k}+\mathbf{q}}^{n\mathbf{k},\nu\mathbf{q}}$  from  $\{|m\mathbf{k} + \mathbf{q}\rangle\}$  to  $\{|n\mathbf{k}\rangle\}$  by emitting a phonon. The transition rate at equilibrium, which is the transition per unit time is given by

$$\Pi_{n\mathbf{k},\nu\mathbf{q}}^{m\mathbf{k}+\mathbf{q}} = \Pi_{m\mathbf{k}+\mathbf{q}}^{n\mathbf{k},\nu\mathbf{q}} = f_{n\mathbf{k}}^0 (1 - f_{m\mathbf{k}+\mathbf{q}}^0) N_{\nu\mathbf{q}}^0 W_{n\mathbf{k},\nu\mathbf{q}}^{m\mathbf{k}+\mathbf{q}} . \quad (65)$$

By writing the canonical form of the scattering term [89] of the BTE for the case of el-ph coupling

$$\frac{\partial f_{n\mathbf{k}}}{\partial t} \Big|_{scatt} = - \sum_{\nu\mathbf{q}} \left( \Pi_{n\mathbf{k},\nu\mathbf{q}}^{m\mathbf{k}+\mathbf{q}} + \Pi_{n\mathbf{k}}^{m\mathbf{k}+\mathbf{q},-\nu\mathbf{q}} \right) (\chi_{n\mathbf{k}} - \chi_{m\mathbf{k}+\mathbf{q}}) \quad (66)$$

where  $\chi_{n\mathbf{k}} = \frac{f_{n\mathbf{k}} - f_{n\mathbf{k}}^0}{f_{n\mathbf{k}}^0(1-f_{n\mathbf{k}}^0)} = \frac{q\mathbf{E}}{k_B T} \cdot \mathbf{G}_{n\mathbf{k}}$  and

$$\Pi_{n\mathbf{k}}^{m\mathbf{k}+\mathbf{q},-\nu\mathbf{q}} = \frac{2\pi}{\hbar} |g_{n\mathbf{k},\nu\mathbf{q}}^{m\mathbf{k}+\mathbf{q}}|^2 f_{n\mathbf{k}}^0 (1 - f_{m\mathbf{k}+\mathbf{q}}^0) (1 + N_{-\nu\mathbf{q}}^0) \delta(\epsilon_{n\mathbf{k}} - \hbar\omega_{-\nu\mathbf{q}} - \epsilon_{m\mathbf{k}+\mathbf{q}}) . \quad (67)$$

In the steady-state and approximating the drift term by keeping only the linear terms in  $\mathbf{E}$ , the BTE can be linearized as [114]

$$\mathbf{v}_{n\mathbf{k}} f_{n\mathbf{k}}^0 (1 - f_{n\mathbf{k}}^0) + \sum_{m,\nu\mathbf{q}} \left( \Pi_{n\mathbf{k},\nu\mathbf{q}}^{m\mathbf{k}+\mathbf{q}} + \Pi_{n\mathbf{k}}^{m\mathbf{k}+\mathbf{q},-\nu\mathbf{q}} \mathbf{G}_{m\mathbf{k}+\mathbf{q}} \right) = \sum_{m,\nu\mathbf{q}} \left( \Pi_{n\mathbf{k},\nu\mathbf{q}}^{m\mathbf{k}+\mathbf{q}} + \Pi_{n\mathbf{k}}^{m\mathbf{k}+\mathbf{q},-\nu\mathbf{q}} \mathbf{G}_{n\mathbf{k}} \right) . \quad (68)$$

The relaxation time approximation is reached when the left hand side summation is neglected and then  $\mathbf{G}_{n\mathbf{k}}^\tau = \mathbf{v}_{n\mathbf{k}} \cdot \tau_{n\mathbf{k}}$ , where  $\tau_{n\mathbf{k}}$  is given by Eq. (46). Alternatively, Eq. (68) can be solved by starting with the RTA solution as an initial guess,  $\mathbf{G}_{n\mathbf{k}}^0 = \mathbf{G}_{n\mathbf{k}}^\tau$ , and iterating using the following relation:

$$\mathbf{G}_{n\mathbf{k}}^{i+1} = \mathbf{G}_{n\mathbf{k}}^0 + \frac{\tau_{n\mathbf{k}}}{f_{n\mathbf{k}}^0(1-f_{n\mathbf{k}}^0)} \left( \Pi_{n\mathbf{k},\nu\mathbf{q}}^{m\mathbf{k}+\mathbf{q}} + \Pi_{n\mathbf{k}}^{m\mathbf{k}+\mathbf{q},-\nu\mathbf{q}} \mathbf{G}_{m\mathbf{k}+\mathbf{q}}^i \right) . \quad (69)$$

This iterative approach has been implemented in ShengBTE code [158] for the solution of BTE for phonons to calculate thermal transport, and for both charge carriers and phonons in Phoebe[155].

#### IV. NUMERICAL APPROACHES AND POST-PROCESSING

In practice, the calculations of TE transport properties on the basis of RTA-BTE can be performed using different levels of approximation with increasing computational cost. The constant relaxation time approximation (CRTA)[159] or methods based on the deformation potential approximation (DPA),[160] have been used extensively.[91, 161–163] The CRTA is generally a poor choice to describe properties other than the Seebeck coefficient due to the lack of el-ph information, and DPA methods fail drastically for materials presenting strong polar optical phonon scattering or inter-band scatterings. Thus, full first-principles calculations of el-ph coupling is necessary in order to obtain accurate TE transport properties.

Even after the sum over phonon modes and integration over the phonon BZ, the el-ph RTs in Eq. (46) are a rich source of microscopic information since they are resolved for different bands and  $\mathbf{k}$ -points. However, calculation of macroscopic transport properties requires a further sum over electron bands and integration over the electron BZ. In order to converge the double BZ integration, very dense  $\mathbf{k}$  and  $\mathbf{q}$  meshes are needed, since the denominator of the integrand may exhibit significant fluctuations on the scale of the phonon energy. For example, calculated mobilities for Si required  $120 \times 120 \times 120$   $\mathbf{k}/\mathbf{q}$  final meshes in order to reach a convergence criterion of  $10^{-4}$  [164]. Direct calculation of such dense meshes is impractical with DFPT, so different interpolation schemes have been developed[106, 114, 165, 166]. Here we briefly review the Wannier-Fourier (WF) and Dual Interpolation approaches.

There are alternative approaches that attempt to reduce the computational cost of el-ph calculations: Samsonidze and Kozinsky proposed the el-ph averaged (EPA) approximation to be used mostly for isotropic materials[167], while Deng *et al.* proposed an approach using a generalized Eliashberg function for short-range el-ph coupling and analytical expressions for long-range el-ph and e-d scatterings[168]. Such methods, along with the development of efficient interpolation schemes, facilitate automated and unsupervised predictions of novel functional materials for thermoelectric or other electronic applications via high-throughput screening.[162, 167–169]

### A. Interpolation schemes

WF interpolation was introduced by Giustino, Cohen and Louie [165] and is based on maximally localized Wannier functions (MLWF) [30] and is analogous to the strategy developed for getting phonon dispersion relations using the interatomic force constants [116]. Within this approach, electronic band structure, phononic dispersions, and el-ph matrix elements,  $g(\mathbf{k}, \mathbf{q})$ , calculated using DFT and DFPT on coarse  $\mathbf{k}, \mathbf{q}$  grids, are interpolated onto much finer  $\mathbf{k}', \mathbf{q}'$  grids through simple matrix multiplications [165]. The el-ph matrix elements on the fine grid are given by

$$g(\mathbf{k}', \mathbf{q}') = \frac{1}{N_e} \sum_{\mathbf{R}_e, \mathbf{R}_p} e^{i(\mathbf{k}' \cdot \mathbf{R}_e + \mathbf{q}' \cdot \mathbf{R}_p)} \mathbf{U}_{\mathbf{k}' + \mathbf{q}'} g(\mathbf{R}_e, \mathbf{R}_p) \mathbf{U}_{\mathbf{k}'}^\dagger \mathbf{u}_{\mathbf{q}'}, \quad (70)$$

where  $\mathbf{R}_e$  and  $\mathbf{R}_p$  are primitive lattice vectors of the Wigner-Seitz (WS) supercell with Born-von-Kármán periodic boundary conditions and  $\mathbf{U}_{\mathbf{k}'}$  ( $\mathbf{u}_{\mathbf{q}'}$ ) are diagonalizer matrices over  $\mathbf{k}'$

$(\mathbf{q}')$  indices from Wannier to Bloch representations for electrons (phonons). The el-ph matrix elements in the real-space Wannier representation are

$$g(\mathbf{R}_e, \mathbf{R}_p) = \frac{1}{N_p} \sum_{\mathbf{k}, \mathbf{q}} e^{-i(\mathbf{k} \cdot \mathbf{R}_e + \mathbf{q} \cdot \mathbf{R}_p)} \mathbf{U}_{\mathbf{k}+\mathbf{q}}^\dagger g(\mathbf{k}, \mathbf{q}) \mathbf{U}_{\mathbf{k}} \mathbf{u}_{\mathbf{q}}^{-1}, \quad (71)$$

$\mathbf{U}_{\mathbf{k}}$  is an unitary matrix corresponding to the rotation of the corresponding electronic states from Bloch to Wannier representations within the gauge of MLWF and  $\mathbf{u}_{\mathbf{q}}$  is a phonon eigenvector. In the above equations, electron band and phonon branch indices are omitted for simplicity. WF interpolation is implemented in EPW [170] and Perturbo [171] codes and establish the basis on which dual interpolation was developed.

The accuracy of WF interpolation strongly depends on the spatial localization of  $g(\mathbf{R}_e, \mathbf{R}_p)$ , which makes it possible to neglect matrix elements outside the WS supercell generated from the initial coarse BZ mesh. A more detailed analysis suggests  $g(\mathbf{R}_e, \mathbf{R}_p)$  should decay in the variable  $\mathbf{R}_e$  at least as fast as MLWFs. In fact, MLWFs in insulators decay quickly provided 2D and 3D systems present time-reversal symmetry [172]. For metals, localized Wannier functions can be obtained from the disentanglement procedure [173]. For  $\mathbf{R}_e = 0$  the localization depends strongly on the dielectric properties of the material and  $g(0, \mathbf{R}_p)$  decays with  $\mathbf{R}_p$  due to the screened Coulomb interaction of the potential generated by atomic displacement. In particular, metals present short screening lengths based on Friedel oscillations and decay as  $|\mathbf{R}_p|^{-4}$  [174], while nonpolar semiconductors may possess an incomplete screening and decay at the rate of a quadrupole,  $|\mathbf{R}_p|^{-3}$  [38]. For ionic and polar covalent crystals, the interpolation turns to be more intricate since the long-range Fröhlich dipole coupling is a relevant contribution, which decays as  $|\mathbf{R}_p|^{-2}$ , resulting a well-known  $|\mathbf{q}^{-1}|$  divergence in momentum space when  $|\mathbf{q}| \rightarrow 0$  [122]. The WF interpolation scheme developed to treat dipole and also quadrupole interactions will be discussed in the next section.

## B. turboEPW with dual interpolation

The dual interpolation approach was developed recently by several of the present authors [175] and represents an effort to improve the computational performance of WF interpolation. It is based on two sequential interpolations, namely, WF interpolation followed by a Fourier interpolation based on star functions. The implementation, called Turbo-EPW, was

built as an extension of the EPW code [170] in order to make use of the latter's well-tested WF interpolation.

As mentioned previously, the calculation of transport properties requires a double integration over  $\mathbf{k}$  and  $\mathbf{q}$  wave vectors. The idea of dual interpolation is to determine  $g$  over a fine  $\mathbf{q}'$  grid using WF interpolation, and perform the partial integration at each of the  $n_{\bar{\mathbf{k}}}$  *irreducible*  $\mathbf{k}$ -points,  $\bar{\mathbf{k}}_l$ , corresponding to a moderately sized, regular  $\mathbf{k}$ -mesh ( $\mathbf{k}^r$ ). (For reasons of clarity, we start with  $\mathbf{q}'$  integration first, however one can easily switch the order and start with  $\mathbf{k}'$  integration.) In this way we determine a generic transport function,  $f(\bar{\mathbf{k}}_l)$ , already integrated over a fine  $\mathbf{q}'$  grid. The next step is the calculation of  $f$  over the whole BZ with fine  $\mathbf{k}'$  grid using a suitable second interpolation that needs to take into account the symmetry of the crystal. The second interpolation uses symmetry-adapted plane-waves or star functions,  $\Upsilon_m(\mathbf{k}')$ , as a basis set to Fourier expand  $f$  [176]:

$$\tilde{f}(\mathbf{k}') = \sum_{m=1}^M a_m \Upsilon_m(\mathbf{k}') , \quad (72)$$

where  $\Upsilon_m(\mathbf{k}') = \frac{1}{n_s} \sum_{\{v\}} \exp[i(v\mathbf{R}_m) \cdot \mathbf{k}']$ , with the sum running over all  $n_s$  point group symmetry operations  $\{v\}$  of the direct lattice  $\mathbf{R}_m$ .

Following the method first proposed by Shankland-Koelling-Wood [177, 178], the number of star functions in the expansion,  $M$ , is taken to be greater than the number of data points ( $M > n_{\bar{\mathbf{k}}}$ ), and the interpolating function,  $\tilde{f}$ , is required to pass through the data points exactly. The freedom from extra star functions is used to minimize a spline-like roughness functional in order to minimize oscillations between data points. As defined by Pickett, Krakauer and Allen [179], the spline-like roughness functional reads  $\Pi = \sum_{m=2}^M |a_m|^2 \rho(R_m)$  with  $\rho(R_m) = \left(1 - c_1 \left(\frac{R_m}{R_{min}}\right)^2\right)^2 + c_2 \left(\frac{R_m}{R_{min}}\right)^6$ , where  $R_m = |\mathbf{R}_m|$ ,  $R_{min}$  is the magnitude of the smallest nonzero lattice vector, and  $c_1 = c_2 = 3/4$ . The determination of the Fourier coefficients,  $a_m$ , is accomplished by the Lagrange multiplier method once the problem has been reduced to minimizing  $\Pi$  subject to the constraints,  $\tilde{f}(\bar{\mathbf{k}}_l) = f(\bar{\mathbf{k}}_l)$ . The result is

$$a_m = \begin{cases} \rho(R_m)^{-1} \sum_{l=1}^{n_{\bar{\mathbf{k}}}-1} \lambda_l^* [\Upsilon_m^*(\bar{\mathbf{k}}_l) - \Upsilon_m^*(\bar{\mathbf{k}}_{n_{\bar{\mathbf{k}}}})] , & m > 1, \\ f(\bar{\mathbf{k}}_{n_{\bar{\mathbf{k}}}}) - \sum_{m=2}^M a_m \Upsilon_m(\bar{\mathbf{k}}_{n_{\bar{\mathbf{k}}}}) , & m = 1, \end{cases} \quad (73)$$

in which the Lagrange multipliers,  $\lambda_l^*$ , can be evaluated from

$$f(\bar{\mathbf{k}}_p) - f(\bar{\mathbf{k}}_{n_{\bar{\mathbf{k}}}}) = \sum_{l=1}^{n_{\bar{\mathbf{k}}}-1} \mathbf{H}_{pl} \lambda_l^* , \quad (74)$$

with

$$\mathbf{H}_{pl} = \sum_{m=2}^M \frac{[\Upsilon_m(\bar{\mathbf{k}}_p) - \Upsilon_m(\bar{\mathbf{k}}_{n_{\bar{\mathbf{k}}})}] [\Upsilon_m^*(\bar{\mathbf{k}}_l) - \Upsilon_m^*(\bar{\mathbf{k}}_{n_{\bar{\mathbf{k}}})}]}{\rho(R_m)} . \quad (75)$$

The interpolating function  $\tilde{f}$  can be written as a linear mapping of the WF data

$$\tilde{f}(\mathbf{k}') = \sum_{l=1}^{n_{\bar{\mathbf{k}}}-1} J(\bar{\mathbf{k}}_l, \mathbf{k}') [f(\bar{\mathbf{k}}_l) - f(\bar{\mathbf{k}}_{n_{\bar{\mathbf{k}}}})] , \quad (76)$$

where  $J$  is the transformation formula independent of the data. In fact,  $J$  is determined by the set of irreducible sampling points  $(\bar{\mathbf{k}}_l)$ , the number of star functions ( $M$ ), and the form of the roughness functional ( $\Pi$ ):

$$J(\bar{\mathbf{k}}_l, \mathbf{k}') = \sum_{p=1}^{n_{\bar{\mathbf{k}}}-1} \sum_m \frac{[\Upsilon_m^*(\bar{\mathbf{k}}_p) - \Upsilon_m^*(\bar{\mathbf{k}}_{n_{\bar{\mathbf{k}}})}] \Upsilon_m(\mathbf{k}')}{\rho(R_m) \mathbf{H}_{pl}} . \quad (77)$$

Basically,  $J$  transforms  $\bar{\mathbf{k}}_l \rightarrow \mathbf{k}'$ , which allows for great computational savings since the final homogeneous grid ( $\mathbf{k}'$ ) on which  $f$  is calculated can be much larger than the regular grid ( $\mathbf{k}^r$ ) that generated the irreducible points.

In practice, to expand the interpolating function in Eq. (72), we rely on a 3D Fast Fourier Transform (FFT) to reciprocal space of the lattice points and their respective star functions that were generated in real space. We take advantage of the periodic boundary conditions to enlarge the real space by the expansion factor  $M$ , the number of star functions per  $\mathbf{k}$ -point, to get a new homogeneous  $\mathbf{k}'$ -grid much finer than the original one. To take into account crystal anisotropy, the extension of the real space is determined by defining spheres for each crystallographic axis with the maximum radius given in terms of their reciprocal primitive vectors. More details can be found in Ref. 175.

The FFT computational complexity,  $\mathcal{O}(N \log N)$ , where  $N$  corresponds to the number of data points related to the product of FFT dimensions, is more affordable than the computational complexity of classical matrix multiplications ( $\mathcal{O}(N^3)$ ) as performed by single WF interpolation. The overall gain in computational performance by using the dual interpolation method compared to a single WF interpolation is approximately  $2(n_s \times M)$ . As  $M$  typically ranges between 5 and 60, there is a great boost in performance that allows for improved calculations of el-ph mediated transport properties. This method was employed to calculate thermoelectric properties in layered materials, such as SnSe and GeSe and will be reviewed in Sect. V.

### C. Third order force constants

The calculation of lattice thermal conductivity within the BTE framework requires determination of the relevant contributions to the phonon scattering matrix. The primary contribution is the phonon-phonon scattering based on the calculation of third-order force constants. While in principle these could be calculated using DFPT, in practice they are generally determined using the supercell method. Routines within either the `ShengBTE` [158] or `phono3py` [180] packages can be used create the necessary supercells containing strategically displaced atoms that allow for the construction of the third-order force constants after the the total energy DFT calculations for each of the supercells has been completed. Since the number of atomic triplets grows rapidly, a cutoff distance, beyond which atomic interactions are ignored, is generally applied to keep the number of supercell calculations manageable. However, for materials with low thermal conductivity, care must be taken to converge results with respect to the cutoff, since long-range interactions can be important for accurate determinations of the lattice thermal conductivity [181].

### D. Calculating transport coefficients

Once the ingredients for the electron/hole or phonon scattering matrix have been determined, the BTE needs to be solved to find the transport coefficients and properties of interest. Within the RTA the `BoltzTraP` package[159] is frequently employed for determining electron and hole transport properties, while the `ShengBTE` package [158] is often used for phonons to calculate thermal transport. The newer `Phoebe` code[155] seeks to treat both thermal and electrical conduction within a single framework.

## V. APPLICATION TO LAYERED THERMOELECTRIC MATERIALS

### A. Thermoelectric $zT$ optimization

Thermoelectric performance, as measured by the dimensionless figure of merit  $zT = \sigma S^2 T / \kappa_{\text{tot}}$ , is maximized at a given temperature  $T$  in materials with both a high electrical conductivity  $\sigma$  and high Seebeck coefficient  $S$ , along with low total thermal conductivity,  $\kappa_{\text{tot}} = \kappa_{\text{carr}} + \kappa_{\text{latt}}$ , which has contributions from the electrical carriers and the atomic lattice,

respectively. Because the calculation of the thermoelectric figure of merit depends on both electronic and phononic transport properties, it serves as an excellent example of how the above methodologies can be put into practice.

A thermoelectric with a high figure of merit is expected to be a material with a high  $PF$ , where the charge-coupled entropy conductivity is larger than the non-coupling entropy conductivity due to purely irreversible processes. One strategy to increase the  $PF$  is band-structure engineering.[182–186] In order to decrease purely irreversible processes, common strategies focus on the reduction of the lattice thermal conductivity,  $\kappa_{\text{latt}}$ [187–193] with less attention given to  $\kappa_{\text{el}}$ . Given the high carrier concentrations of optimally doped TE materials,  $\kappa_{\text{el}}$  should not be ignored; reducing it can be best accomplished by minimizing the Lorenz number,  $L = \kappa_{\text{el}}/(\sigma T)$ .[194, 195] It is important to note, however, that direct measurements of  $L$  and  $\kappa_{\text{el}}$  are nontrivial. Typically  $\kappa_{\text{el}}$  is estimated based on the Wiedemann–Franz law by using measured values of  $\sigma$  and estimated values of  $L$  from simplified parabolic band approximations.[196, 197] In general such estimations are inaccurate,[194, 198] making first-principles calculations of  $L$  and  $\kappa_{\text{el}}$  necessary.

Despite the complexity arising from the interdependence of all the transport properties that contribute to  $zT$ , the search for high- $zT$  materials continues [199], and new high-performance TE materials are constantly emerging.[200–206] An important class of such materials are the bulk crystals with a two-dimensional (2D) layered structure which have high anisotropy and improved electrical conductivity along in-plane directions.[207–210] (For a review see Li *et al.*[211]) In particular, the extremely high  $zT$  values reported for intrinsic [212], p-doped [213] and n-doped[214] SnSe has boosted the interest in high-efficiency layered TE materials. Significant effort has gone into trying to accurately calculate its properties [133, 181, 215–219], both in order to optimize its performance, but also in the hopes that understanding its fundamental properties will allow for predictions of additional high-performance thermoelectric materials. In that vein, germanium selenide (GeSe) is an obvious isostructural material that has been the focus of only a handful of experimental [220, 221] and theoretical [134, 222–224] studies. The crystal structure of GeSe (SnSe) is shown in Fig. 3, along with the basic electronic and phononic band structures calculated using DFT. Here we discuss calculations of the thermoelectric properties of SnSe and GeSe in comparison with previous calculations and experimental measurements in order to highlight the successes and challenges inherent in a DFT-based first-principles framework for

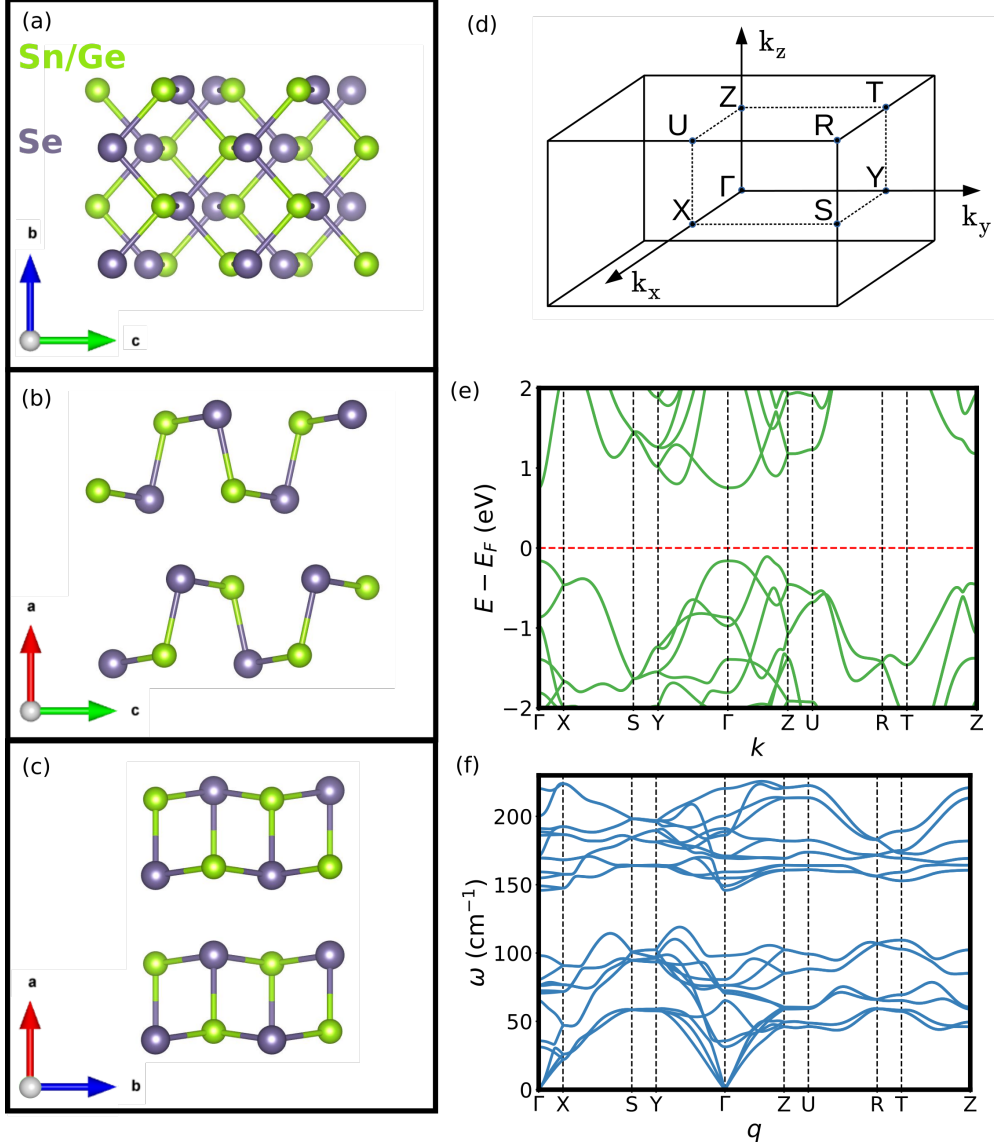


FIG. 3. (a)-(c) GeSe (SnSe) crystal structure along each axis. (d) The Brillouin zone with high symmetry points labeled. (e) Electronic and (f) phononic band structure for GeSe.

calculating thermoelectric performance.

### B. Electronic transport in SnSe and GeSe

Using the above framework for calculating electron-phonon scattering with DFT, our TurboEPW implementation [175] allowed for the sampling of over 1 billion  $\mathbf{k}/\mathbf{q}$  pairs and thus a detailed calculation of the momentum- and band-resolved impurity, polar, and non-polar scattering rates. These scattering rates can be expressed as a function of the carrier energy

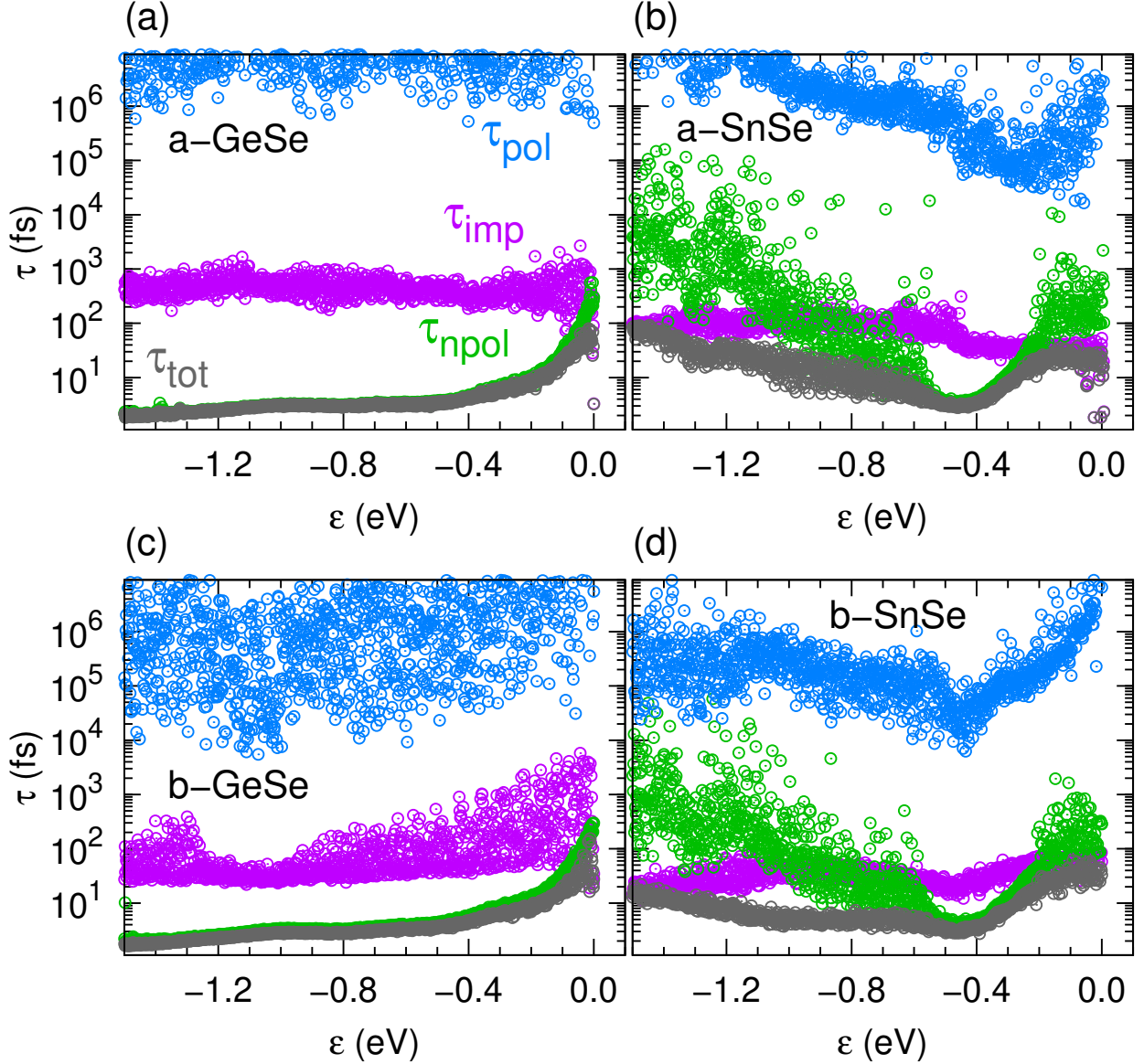


FIG. 4. Energy-resolved scattering times due to polar and non-polar phonons as well as impurities, calculated for the a- and b-axes of SnSe and GeSe. From Ref. 134.

using a velocity-weighted average:

$$\tau(\epsilon) = \frac{\sum_{n,\mathbf{k}} \tau(n, \mathbf{k}) v_{n,\mathbf{k}} v_{n,\mathbf{k}} \delta(\epsilon - \epsilon_{n,\mathbf{k}})}{\sum_{n,\mathbf{k}} v_{n,\mathbf{k}} v_{n,\mathbf{k}} \delta(\epsilon - \epsilon_{n,\mathbf{k}})}, \quad (78)$$

where  $v_{n,\mathbf{k}} = \partial \epsilon_{n,\mathbf{k}} / \partial k$  is the carrier velocity. Scattering times as a function of carrier energy for SnSe and GeSe are shown in Fig. 4, with more detailed discussion provided in Ref. 134.

The `BoltzTraP` package [159] uses the energy-resolved scattering times to determine many transport properties, including the Seebeck coefficient  $S$ , the electrical conductivity  $\sigma$ , and

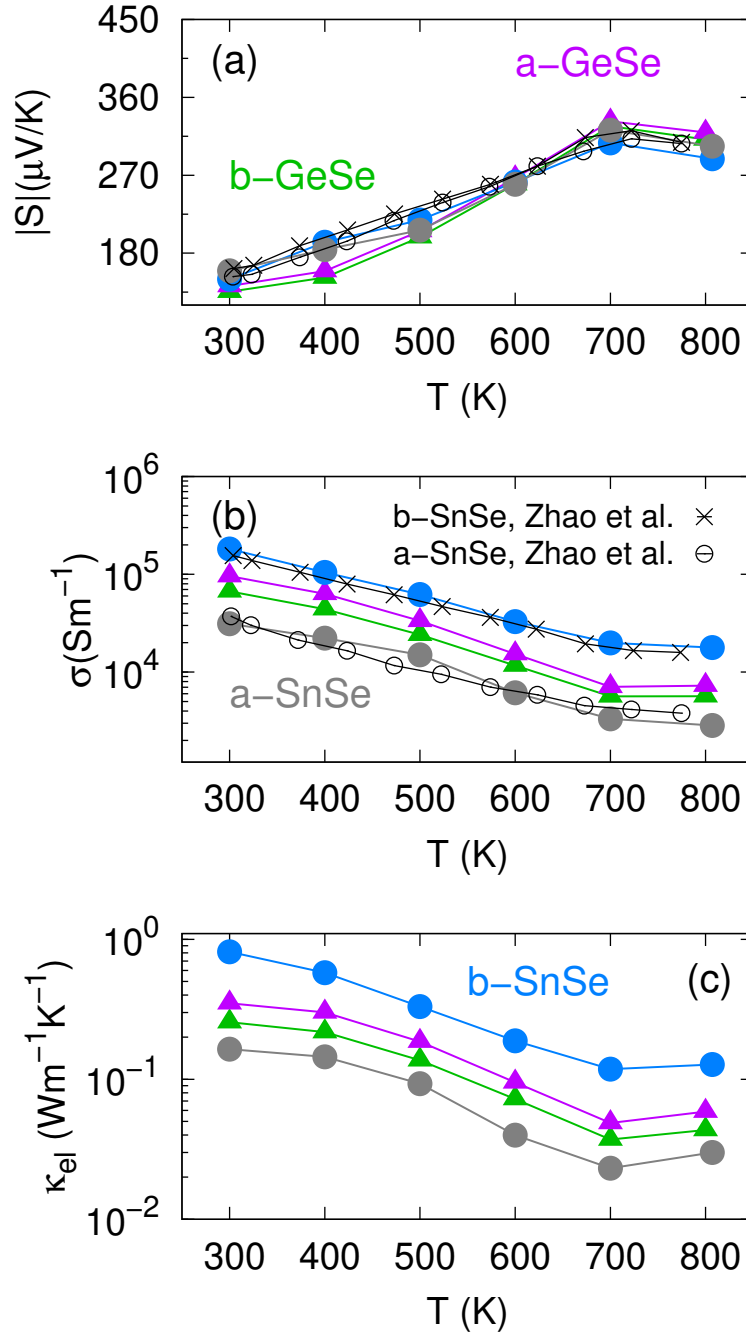


FIG. 5. Thermoelectric transport properties for the a- and b-axes of SnSe and GeSe as a function of temperature, with hole doping concentrations based on experiment.

the carrier thermal conductivity  $\kappa_{\text{carr}}$ , which are needed for predictions of the thermoelectric figure of merit,  $zT$ . Fig. 5 shows these properties as a function of temperature for the *a*- and *b*-axes of SnSe and GeSe with hole doping concentrations based on experimental measurements.[134].

### C. Thermal transport in SnSe and GeSe

The extremely low intrinsic lattice thermal conductivity in single crystal SnSe is a significant contributor to its high figure of merit, so it is natural to hope that GeSe might also exhibit a similarly low  $\kappa_{\text{latt}}$ . The Debye-Callaway framework [222, 225] allows for a simple estimate of  $\kappa_{\text{latt}}$  based on calculations of the second-order force constants needed to determine the phonon spectrum of a crystal. The acoustic phonon velocities and Grüneisen parameters (volume dependence of the phonon frequencies) are used in conjunction with a model for the normal and umklapp scattering rates of acoustic phonons. However, the simplest fully first-principles calculation of  $\kappa_{\text{latt}}$  uses third-order force constants calculated within the harmonic approximation in order to determine the detailed band- and momentum-resolved three-phonon contribution to the scattering matrix for use in the phonon BTE. Additional terms for phonon-isotope, phonon-boundary, and phonon-electron scattering can also be taken into account in the scattering matrix.

Here we discuss the calculation of the thermal conductivity of SnSe and GeSe using an iterative solution to the Boltzman Transport Equation (BTE) [226] including third-order force constants for very distant neighbors in large supercells. We include corrections based on the Wigner distribution [227], which gives small but non-negligible corrections arising from phonon bands that overlap due to their finite linewidths.

We begin with a presentation of our results for the lattice thermal conductivity of SnSe because there is a large body of literature seeking to reconcile different experimental and theoretical results, yielding many sources for comparison. As shown in Fig. 3(a)-(c), the SnSe crystal is highly anisotropic, so the calculated results for  $\kappa_{\text{latt}}$  displayed in Fig. 6(a) are displayed in purple, blue, and green for transport along the a-, b-, and c-axes, respectively. The force constants were calculated using VASP[27, 28] with supercells generated by phono3py[180], while the solution of the BTE and calculation of  $\kappa_{\text{latt}}$  was done with Phoebe[155].

Generally speaking, calculations predict a very low thermal conductivity for SnSe, but not quite as low as the initial measurements on single crystals [212], which were surprising because they were even lower than previous measurements on polycrystalline samples, which one would expect to have lower thermal conductivity due to increased boundary scattering. Subsequent work has suggested that careful removal of SnO residue from polycrystalline

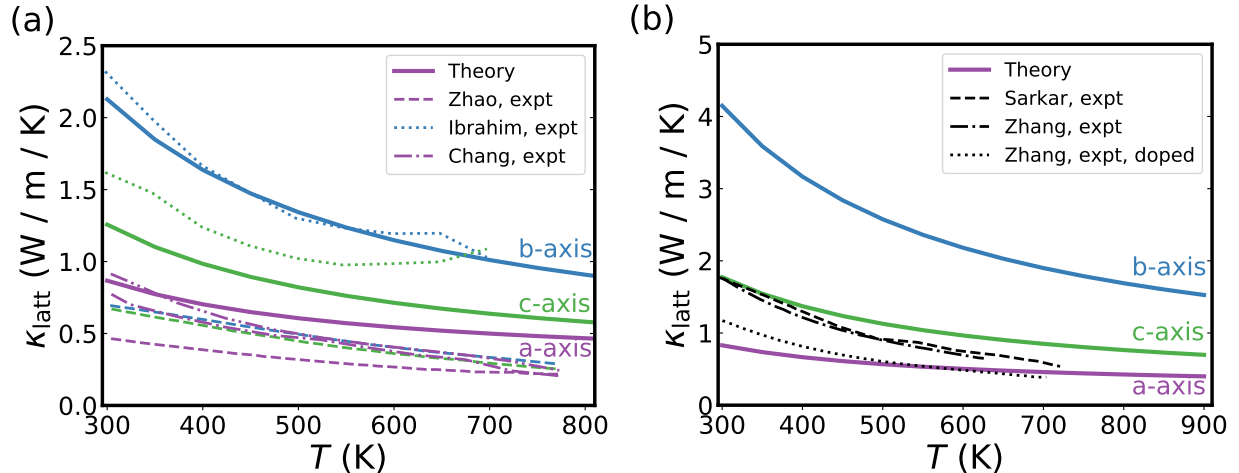


FIG. 6. Calculated lattice thermal conductivity along each axis as a function of temperature, compared to published experimental measurements for (a) SnSe and (b) GeSe. Experimental SnSe measurements are from Zhao [213], Ibrahim [229], and Chang [214] while GeSe measurements are from from Sarkar [230] (polycrystalline) and Zhang [220] (polycrystalline GeSe without and with 3% Ag doping).

samples can reduce its thermal conductivity [228]. In Fig. 6(a) our predictions are compared to several experimental measurements of both undoped and doped samples. While there is obviously not perfect agreement (even between experimental measurements), it is clear that the calculations are giving a reasonable estimate for the extremely low thermal conductivity of SnSe, especially if considered in the context of other insulators that have thermal conductivities that are orders of magnitude larger.

Turning now to GeSe, Fig. 6(b) shows our calculated results for  $\kappa_{\text{latt}}$  in comparison to several experimental results. Previous calculations based on the Debye-Callaway theory predict extremely low values of  $\kappa_{\text{latt}}$ , well below 1 W/m/K for all three axes [222]. Our results, based on the methodology described above, yield values significantly higher and qualitatively different from those based on Debye-Callaway theory, but similar to previous calculations also based on third-order force constants [224], but without the inclusion of the Wigner correction. In particular, a very high level of anisotropy is predicted, with the *b*-axis  $\kappa_{\text{latt}}$  roughly double the value for *c*-axis, which is in turn roughly double the *a*-axis value, all at 300 K.

Calculations of lattice thermal conductivity, particularly for systems with significant an-

harmonicity, remain quite challenging. Within a specific framework it is essential to thoroughly converge the results with respect to the various computational parameters, such as supercell size, cutoff radius, DFT settings, and q-grid for the BTE, to list some examples relevant to above examples. However, different levels of theory can lead to significant variations in the results, without an *a priori* means of gauging accuracy with respect to experiment. For instance, in a study of PbTe [231] the authors found that finite temperature phonon frequency shifts increased the lattice thermal conductivity, but the addition of 4-phonon scattering reduced the thermal conductivity. This is a case where accidental cancellation between higher-order contributions allowed simpler models to fortuitously agree well with experiment. The calculations and even experimental measurements of  $\kappa_{\text{latt}}$  for SnSe are also not simple and not without controversy [229, 232–234], and significant effort has been put into increasing the sophistication of theoretical calculations by including, among other approaches, non-perturbative anharmonic effects [219].

Nevertheless, comparisons between different materials at the same level of theory can still give some important physical insight. Comparing the two panels of Fig. 6 we see that while the thermal conductivity along the  $a$ -axis is nearly identical for SnSe and GeSe, the latter exhibits slightly higher thermal conductivities along the  $b$ - and  $c$ -axis. Averaging over the three axes, as would be relevant for polycrystalline samples, the GeSe thermal conductivity is roughly 50% larger than SnSe throughout the temperature range studied. There has been recent success purifying polycrystalline SnSe to remove tin oxides [228, 235], revealing the intrinsic lattice thermal conductivity that matches more closely the experimental measurements on single crystal samples, in particular along the lowest conductivity  $a$ -axis. This gives good reason to hope that polycrystalline GeSe samples with comparably low lattice thermal conductivity can be synthesized in the near future.

#### D. Thermoelectric figure of merit in SnSe and GeSe

The calculations of carrier transport can be combined with those of lattice thermal conductivity to make predictions for the thermoelectric figure of merit,  $zT$ . The thermal conductivity due to hole transport,  $\kappa_{\text{carr}}$ , was calculated using a first-principles framework [91, 133] where the material dependent carrier concentration ( $n_{\text{carr}}$ ) and ionized impurity concentration ( $n_{\text{ii}}$ ) were determined in a self-consistent manner so that calculated values of the Seebeck

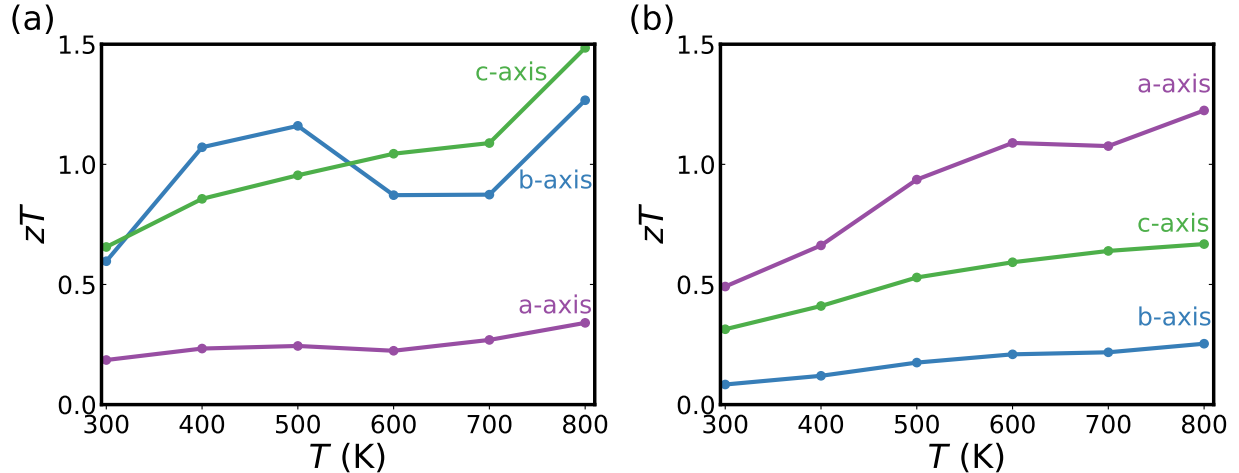


FIG. 7. Calculated thermoelectric figure of merit  $zT = \sigma S^2 T / \kappa_{\text{tot}}$  for each axis of hole-doped (a) SnSe and (b) GeSe, where all transport properties are calculated from first principles using carrier and impurity concentrations derived self-consistently from data for *a*-axis SnSe [233].

coefficient,  $S$ , and electrical conductivity,  $\sigma$ , matched experimental measurements in actual *p*-doped SnSe samples [233]. The temperature dependent carrier and impurity concentrations in SnSe were then used as a realistic approximation for the same quantities in GeSe, allowing for calculations of hole transport properties in GeSe under potential experimental conditions.

The ultimate goal is discover practical thermoelectric materials, so in Fig. 7 we show the calculations of lattice thermal conductivity with the carrier transport properties described in the previous paragraph, yielding a prediction for the thermoelectric figure of merit,  $zT = \sigma S^2 T / \kappa_{\text{tot}}$ , along each of the axes of SnSe and GeSe. The values of  $\kappa_{\text{tot}}$  presented here are higher than those based on the Debye-Callaway model, leading to less optimistic predictions for  $zT$ . Nevertheless, GeSe exhibits significant thermoelectric potential, especially along the *a*-axis. This is in contrast to a previous prediction based on similar lattice thermal conductivity results but a simpler model for the carrier contributions, which yielded significantly lower  $zT$  along the *a*-axis in comparison to the *c*-axis [224]. Because our prediction is based on specific, realistic values of carrier and impurity concentrations, one can reasonably hope that by optimizing of the doping concentration the values of  $zT$  can be improved[134]. Furthermore, polycrystalline samples of GeSe should, with proper care for purity and removal of oxides, yield equivalent or even lower thermal conductivities,

and consequently even greater potential for a high figure of merit.

## VI. CONCLUSIONS

We have outlined how, starting from the fundamental quantum mechanical Hamiltonian for a periodic crystal of nuclei and electrons, one can leverage modern high performance computing infrastructure to calculate a macroscopic property of significant technical importance such as the thermoelectric figure of merit,  $zT$ . The well-established framework of Kohn-Sham DFT converts the  $N$ -body Hamiltonian eigenvalue problem into a self-consistent numerical optimization problem for single-particle orbitals. This allows for the extraction of the electron-phonon and phonon-phonon couplings that determine the relevant scattering mechanisms that serve as input to the Boltzmann Transport Equation. The electron and phonon distribution functions determined by the BTE can then be used to calculate all the necessary experimental observables that go into the calculation of  $zT$ . As a demonstration of this process we focused on the thermoelectric performance of hole-doped SnSe and GeSe. We have presented calculations of both the electronic transport properties (previously published in Refs. 133, 134) along with new calculations of the phonon lattice thermal conductivity and the resultant predictions for  $zT$ .

## ACKNOWLEDGMENTS

The calculations performed for this work used resources of the National Energy Research Scientific Computing Center (NERSC), a U.S. Department of Energy Office of Science User Facility located at Lawrence Berkeley National Laboratory, operated under Contract No. DE-AC02-05CH11231, as well as the FASRC Cannon cluster supported by the FAS Division of Science Research Computing Group at Harvard University. M.P. is supported by the Swiss National Science Foundation (SNSF) through the Early Postdoc.Mobility program (Grant No. P2ELP2-191706).

---

[1] L. Yang, Z.-G. Chen, M. S. Dargusch, and J. Zou, High performance thermoelectric materials: progress and their applications, *Advanced Energy Materials* **8**, 1701797 (2018).

- [2] F. Giustino, *Materials Modelling Using Density Functional Theory: Properties and Predictions* (Oxford University Press, 2014).
- [3] A. Szabo and N. S. Ostlund, *Modern Quantum Chemistry. Introduction to Advanced Electronic Structure Theory* (Dover, 1996).
- [4] P. Hohenberg and W. Kohn, Inhomogeneous electron gas, [Physical Review](#) **136**, B864 (1964).
- [5] W. Kohn and L. J. Sham, Self-consistent equations including exchange and correlation effects, [Physical Review](#) **140**, A1133 (1965).
- [6] D. Sholl and J. A. Steckel, *Density Functional Theory: A Practical Introduction* (John Wiley & Sons, 2009).
- [7] R. G. Parr and W. Yang, *Density-Functional Theory of Atoms and Molecules* (Oxford University Press, 1994).
- [8] D. M. Ceperley and B. J. Alder, Ground state of the electron gas by a stochastic method, [Physical Review Letters](#) **45**, 566 (1980).
- [9] J. P. Perdew, K. Burke, and M. Ernzerhof, Generalized gradient approximation made simple, [Physical Review Letters](#) **77**, 3865 (1996).
- [10] J. P. Perdew and Y. Wang, Accurate and simple analytic representation of the electron-gas correlation energy, [Physical Review B](#) **45**, 13244 (1992).
- [11] J. P. Perdew, A. Ruzsinszky, G. I. Csonka, O. A. Vydrov, G. E. Scuseria, L. A. Constantin, X. Zhou, and K. Burke, Restoring the density-gradient expansion for exchange in solids and surfaces, [Physical Review Letters](#) **100**, 136406 (2008).
- [12] Y. Zhang and W. Yang, Comment on “Generalized gradient approximation made simple”, [Physical Review Letters](#) **80**, 890 (1998).
- [13] J. Sun, M. Marsman, G. I. Csonka, A. Ruzsinszky, P. Hao, Y.-S. Kim, G. Kresse, and J. P. Perdew, Self-consistent meta-generalized gradient approximation within the projector-augmented-wave method, [Physical Review B](#) **84**, 035117 (2011).
- [14] J. Sun, A. Ruzsinszky, and J. P. Perdew, Strongly constrained and appropriately normed semilocal density functional, [Physical Review Letters](#) **115**, 036402 (2015).
- [15] J. P. Perdew, M. Ernzerhof, and K. Burke, Rationale for mixing exact exchange with density functional approximations, [The Journal of Chemical Physics](#) **105**, 9982 (1996).
- [16] J. Heyd, G. E. Scuseria, and M. Ernzerhof, Hybrid functionals based on a screened Coulomb potential, [The Journal of Chemical Physics](#) **118**, 8207 (2003).

- [17] A. V. Krukau, O. A. Vydrov, A. F. Izmaylov, and G. E. Scuseria, Influence of the exchange screening parameter on the performance of screened hybrid functionals, *The Journal of Chemical Physics* **125**, 224106 (2006).
- [18] A. Görling, Density-functional theory for excited states, *Physical Review A* **54**, 3912 (1996).
- [19] A. J. Cohen, P. Mori-Sánchez, and W. Yang, Insights into current limitations of density functional theory, *Science* **321**, 792 (2008).
- [20] D. Vanderbilt, Soft self-consistent pseudopotentials in a generalized eigenvalue formalism, *Physical Review B* **41**, 7892 (1990).
- [21] D. R. Hamann, M. Schlüter, and C. Chiang, Norm-conserving pseudopotentials, *Physical Review Letters* **43**, 1494 (1979).
- [22] X. Gonze, B. Amadon, P.-M. Anglade, J.-M. Beuken, F. Bottin, P. Boulanger, F. Bruneval, D. Caliste, R. Caracas, M. Côté, T. Deutsch, L. Genovese, P. Ghosez, M. Giantomassi, S. Goedecker, D. Hamann, P. Hermet, F. Jollet, G. Jomard, S. Leroux, M. Mancini, S. Mazzevet, M. Oliveira, G. Onida, Y. Pouillon, T. Rangel, G.-M. Rignanese, D. Sangalli, R. Shaltaf, M. Torrent, M. Verstraete, G. Zerah, and J. Zwanziger, Abinit: First-principles approach to material and nanosystem properties, *Computer Physics Communications* **180**, 2582 (2009).
- [23] S. J. Clark, M. D. Segall, C. J. Pickard, P. J. Hasnip, M. I. J. Probert, K. Refson, and M. C. Payne, First principles methods using castep, *Zeitschrift für Kristallographie - Crystalline Materials* **220**, 567 (2005).
- [24] J. Enkovaara, C. Rostgaard, J. J. Mortensen, J. Chen, M. Dułak, L. Ferrighi, J. Gavnholt, C. Glinsvad, V. Haikola, H. A. Hansen, H. H. Kristoffersen, M. Kuisma, A. H. Larsen, L. Lehtovaara, M. Ljungberg, O. Lopez-Acevedo, P. G. Moses, J. Ojanen, T. Olsen, V. Petzold, N. A. Romero, J. Stausholm-Møller, M. Strange, G. A. Tritsaris, M. Vanin, M. Walter, B. Hammer, H. Häkkinen, G. K. H. Madsen, R. M. Nieminen, J. K. Nørskov, M. Puska, T. T. Rantala, J. Schiøtz, K. S. Thygesen, and K. W. Jacobsen, Electronic structure calculations with GPAW: a real-space implementation of the projector augmented-wave method, *Journal of Physics: Condensed Matter* **22**, 253202 (2010).
- [25] J. C. Prentice, J. Aarons, J. C. Womack, A. E. Allen, L. Andrinopoulos, L. Anton, R. A. Bell, A. Bhandari, G. A. Bramley, R. J. Charlton, *et al.*, The onetep linear-scaling density functional theory program, *The Journal of Chemical Physics* **152**, 174111 (2020).

[26] P. Giannozzi, S. Baroni, N. Bonini, M. Calandra, R. Car, C. Cavazzoni, D. Ceresoli, G. L. Chiarotti, M. Cococcioni, I. Dabo, A. D. Corso, S. de Gironcoli, S. Fabris, G. Fratesi, R. Gebauer, U. Gerstmann, C. Gougoussis, A. Kokalj, M. Lazzeri, L. Martin-Samos, N. Marzari, F. Mauri, R. Mazzarello, S. Paolini, A. Pasquarello, L. Paulatto, C. Sbraccia, S. Scandolo, G. Sclauzero, A. P. Seitsonen, A. Smogunov, P. Umari, and R. M. Wentzcovitch, QUANTUM ESPRESSO: a modular and open-source software project for quantum simulations of materials, *Journal of Physics: Condensed Matter* **21**, 395502 (2009).

[27] G. Kresse and J. Furthmüller, Efficient iterative schemes for *ab initio* total-energy calculations using a plane-wave basis set, *Phys. Rev. B* **54**, 11169 (1996).

[28] G. Kresse and J. Furthmüller, Efficiency of *ab-initio* total energy calculations for metals and semiconductors using a plane-wave basis set, *Computational Materials Science* **6**, 15 (1996).

[29] Besides plane waves, localized basis sets consisting of atomic-like orbitals (e.g., Gaussian- or Slater-type functions) have found a widespread use, in particular in the computational chemistry community. Contrary to plane waves, fewer basis functions are often needed to achieve a reasonable accuracy, hence significantly decreasing the computational effort. However, localized basis sets are controlled by many parameters in addition to the energy cutoff, in a way that no systematic convergence can be attained.

[30] N. Marzari and D. Vanderbilt, Maximally localized generalized wannier functions for composite energy bands, *Physical Review B* **56**, 12847 (1997).

[31] N. Marzari, A. A. Mostofi, J. R. Yates, I. Souza, and D. Vanderbilt, Maximally localized wannier functions: Theory and applications, *Review of Modern Physics* **84**, 1419 (2012).

[32] A. A. Mostofi, J. R. Yates, Y.-S. Lee, I. Souza, D. Vanderbilt, and N. Marzari, wannier90: A tool for obtaining maximally-localised wannier functions, *Computer Physics Communications* **178**, 685 (2008).

[33] A. A. Mostofi, J. R. Yates, G. Pizzi, Y.-S. Lee, I. Souza, D. Vanderbilt, and N. Marzari, An updated version of wannier90: A tool for obtaining maximally-localised wannier functions, *Computer Physics Communications* **185**, 2309 (2014).

[34] M. Born and K. Huang, *Dynamical theory of crystal lattices* (Clarendon Press, 1966).

[35] H. Hellmann, *Einführung in die Quantenchemie* (F. Deuticke, Leipzig, 1937).

[36] R. P. Feynman, Forces in molecules, *Physical Review* **56**, 340 (1939).

[37] P. DeCicco and F. Johnson, The quantum theory of lattice dynamics. IV, *Proceedings of the Royal Society of London. A. Mathematical and Physical Sciences* **310**, 111 (1969).

[38] R. M. Pick, M. H. Cohen, and R. M. Martin, Microscopic theory of force constants in the adiabatic approximation, *Physical Review B* **1**, 910 (1970).

[39] A. A. Maradudin and S. H. Vosko, Symmetry properties of the normal vibrations of a crystal, *Reviews of Modern Physics* **40**, 1 (1968).

[40] S. Baroni, P. Giannozzi, and A. Testa, Elastic constants of crystals from linear-response theory, *Physical Review Letters* **59**, 2662 (1987).

[41] Z. H. Levine and D. C. Allan, Linear optical response in silicon and germanium including self-energy effects, *Physical Review Letters* **63**, 1719 (1989).

[42] P. Giannozzi, S. De Gironcoli, P. Pavone, and S. Baroni, *Ab initio* calculation of phonon dispersions in semiconductors, *Physical Review B* **43**, 7231 (1991).

[43] S. de Gironcoli, S. Baroni, and R. Resta, Piezoelectric properties of III-V semiconductors from first-principles linear-response theory, *Physical Review Letters* **62**, 2853 (1989).

[44] S. de Gironcoli, P. Giannozzi, and S. Baroni, Structure and thermodynamics of  $\text{Si}_x \text{Ge}_{1-x}$  alloys from *ab initio* monte carlo simulations, *Physical Review Letters* **66**, 2116 (1991).

[45] A. Dal Corso, S. Baroni, and R. Resta, Density-functional theory of the dielectric constant: Gradient-corrected calculation for silicon, *Physical Review B* **49**, 5323 (1994).

[46] A. A. Quong and A. G. Eguiluz, First-principles evaluation of dynamical response and plasmon dispersion in metals, *Physical Review Letters* **70**, 3955 (1993).

[47] M. Stengel, Flexoelectricity from density-functional perturbation theory, *Physical Review B* **88**, 174106 (2013).

[48] C. E. Dreyer, M. Stengel, and D. Vanderbilt, Current-density implementation for calculating flexoelectric coefficients, *Physical Review B* **98**, 075153 (2018).

[49] M. Royo and M. Stengel, First-principles theory of spatial dispersion: Dynamical quadrupoles and flexoelectricity, *Physical Review X* **9**, 021050 (2019).

[50] M. Stott and E. Zaremba, Linear-response theory within the density-functional formalism: Application to atomic polarizabilities, *Physical Review A* **21**, 12 (1980).

[51] A. Zangwill and P. Soven, Resonant photoemission in barium and cerium, *Physical Review Letters* **45**, 204 (1980).

- [52] G. Mahan, Modified Sternheimer equation for polarizability, *Physical Review A* **22**, 1780 (1980).
- [53] S. K. Ghosh and B. M. Deb, Dynamic polarizability of many-electron systems within a time-dependent density-functional theory, *Chemical Physics* **71**, 295 (1982).
- [54] N. Zein, On density functional calculations of crystal elastic modula and phonon spectra, *Fizika Tverdogo Tela* **26**, 3028 (1984).
- [55] S. Baroni, P. Giannozzi, and A. Testa, Green's-function approach to linear response in solids, *Physical Review Letters* **58**, 1861 (1987).
- [56] X. Gonze, D. C. Allan, and M. P. Teter, Dielectric tensor, effective charges, and phonons in  $\alpha$ -quartz by variational density-functional perturbation theory, *Physical Review Letters* **68**, 3603 (1992).
- [57] X. Gonze and J.-P. Vigneron, Density-functional approach to nonlinear-response coefficients of solids, *Physical Review B* **39**, 13120 (1989).
- [58] J. O. Hirschfelder, W. B. Brown, and S. T. Epstein, Recent developments in perturbation theory, in *Advances in Quantum Chemistry* (Academic Press Inc., 1964) pp. 255–374.
- [59] S. Baroni, S. De Gironcoli, A. Dal Corso, and P. Giannozzi, Phonons and related crystal properties from density-functional perturbation theory, *Reviews of Modern Physics* **73**, 515 (2001).
- [60] X. Gonze, Adiabatic density-functional perturbation theory, *Physical Review A* **52**, 1096 (1995).
- [61] X. Gonze, Perturbation expansion of variational principles at arbitrary order, *Physical Review A* **52**, 1086 (1995).
- [62] P. K. Lam and M. L. Cohen, *Ab initio* calculation of phonon frequencies of Al, *Physical Review B* **25**, 6139 (1982).
- [63] A. Togo, First-principles phonon calculations with phonopy and phono3py, *Journal of the Physical Society of Japan* **92**, 012001 (2023).
- [64] A. J. McGaughey and M. Kaviany, Phonon transport in molecular dynamics simulations: formulation and thermal conductivity prediction, *Advances in Heat Transfer* **39**, 169 (2006).
- [65] L. T. Kong, Phonon dispersion measured directly from molecular dynamics simulations, *Computer Physics Communications* **182**, 2201 (2011).

[66] H. Haug, A.-P. Jauho, and M. Cardona, *Quantum kinetics in transport and optics of semiconductors*, Vol. 2 (Springer, 2008).

[67] G. Stefanucci and R. Van Leeuwen, *Nonequilibrium many-body theory of quantum systems: a modern introduction* (Cambridge University Press, 2013).

[68] G. D. Mahan, Condensed matter in a nutshell, in *Condensed Matter in a Nutshell* (Princeton University Press, 2010).

[69] R. Kubo, Statistical-mechanical theory of irreversible processes. I. general theory and simple applications to magnetic and conduction problems, *Journal of the Physical Society of Japan* **12**, 570 (1957).

[70] R. Kubo, The fluctuation-dissipation theorem, *Reports on Progress in Physics* **29**, 255 (1966).

[71] D. Thouless, Relation between the Kubo-Greenwood formula and the Boltzmann equation for electrical conductivity, *Philosophical Magazine* **32**, 877 (1975).

[72] S. Poncé, W. Li, S. Reichardt, and F. Giustino, First-principles calculations of charge carrier mobility and conductivity in bulk semiconductors and two-dimensional materials, *Reports on Progress in Physics* **83**, 036501 (2020).

[73] D. Sangalli and A. Marini, Ultra-fast carriers relaxation in bulk silicon following photo-excitation with a short and polarized laser pulse, *EPL (Europhysics Letters)* **110**, 47004 (2015).

[74] L. Landau, On the theory of the fermi liquid, *Sov. Phys. JETP* **8**, 70 (1959).

[75] D. Pines, *Theory of Quantum Liquids: Normal Fermi Liquids* (CRC Press, 2018).

[76] N. Pottier, *Nonequilibrium statistical physics: linear irreversible processes* (Oxford University Press, 2009).

[77] R. Peierls, Some simple remarks on the basis of transport theory, in *Transport Phenomena* (Springer, 1974) pp. 1–33.

[78] N. E. Hussey, K. Takenaka, and H. Takagi, Universality of the Mott–Ioffe–Regel limit in metals, *Philosophical Magazine* **84**, 2847 (2004).

[79] V. J. Emery and S. A. Kivelson, Superconductivity in bad metals, *Physical Review Letters* **74**, 3253 (1995).

[80] S. A. Hartnoll, Theory of universal incoherent metallic transport, *Nature Physics* **11**, 54 (2015).

[81] W. Kohn and J. M. Luttinger, Quantum theory of electrical transport phenomena, *Physical Review* **108**, 590 (1957).

[82] J. M. Luttinger and W. Kohn, Quantum theory of electrical transport phenomena. II, *Physical Review* **109**, 1892 (1958).

[83] D. Xiao, M.-C. Chang, and Q. Niu, Berry phase effects on electronic properties, *Reviews of Modern Physics* **82**, 1959 (2010).

[84] J. von Neumann, Proof of the ergodic theorem and the H-theorem in quantum mechanics, *The European Physical Journal H* **35**, 201 (2010).

[85] L. P. Kadanoff, Entropy is in flux V3.4, *Journal of Statistical Physics* **167**, 1039 (2017).

[86] P. Allen, Boltzmann theory and resistivity of metals, *Kluwer International Series In Engineering And Computer Science* , 219 (1996).

[87] S. Poncé, E. R. Margine, and F. Giustino, Towards predictive many-body calculations of phonon-limited carrier mobilities in semiconductors, *Physical Review B* **97**, 121201 (2018).

[88] Y. Liu, Z. Yuan, R. Wesselink, A. A. Starikov, M. Van Schilfgaarde, and P. J. Kelly, Direct method for calculating temperature-dependent transport properties, *Physical Review B* **91**, 220405 (2015).

[89] J. M. Ziman, *Electrons and phonons: the theory of transport phenomena in solids* (Oxford University Press, 2001).

[90] B. M. Askerov and S. Figarova, *Thermodynamics, Gibbs Method and Statistical Physics of Electron Gases*, Vol. 57 (Springer Science & Business Media, 2009).

[91] A. S. Chaves, R. L. González-Romero, J. J. Meléndez, and A. Antonelli, Investigating charge carrier scattering processes in anisotropic semiconductors through first-principles calculations: The case of p-type SnSe, *Physical Chemistry Chemical Physics* **23**, 900 (2021).

[92] S. Ahmad and S. Mahanti, Energy and temperature dependence of relaxation time and Wiedemann-Franz law on PbTe, *Physical Review B* **81**, 165203 (2010).

[93] Y. I. Ravich, B. Efimova, and V. Tamarchenko, Scattering of current carriers and transport phenomena in lead chalcogenides, *Physica Status Solidi (B)* **43**, 11 (1971).

[94] L. Onsager, Reciprocal relations in irreversible processes. I., *Physical Review* **37**, 405 (1931).

[95] L. Onsager, Reciprocal relations in irreversible processes. II., *Physical Review* **38**, 2265 (1931).

[96] H. B. Callen, The application of Onsager's reciprocal relations to thermoelectric, thermomagnetic, and galvanomagnetic effects, *Physical Review* **73**, 1349 (1948).

[97] S. R. Groot, *Thermodynamics of irreversible processes*, Vol. 3 (North-Holland Publishing Company, 1963).

[98] H. B. Callen, *Thermodynamics and an Introduction to Thermostatistics* (Wiley, 1995).

[99] C. Goupil, W. Seifert, K. Zabrocki, E. Müller, and G. J. Snyder, Thermodynamics of thermoelectric phenomena and applications, *Entropy* **13**, 1481 (2011).

[100] A. Feldhoff, Thermoelectric material tensor derived from the onsager–de groot–callen model, *Energy Harvesting and Systems* **2**, 5 (2015).

[101] P. Chaikin, An introduction to thermopower for those who might want to use it to study organic conductors and superconductors, in *Organic Superconductivity* (Springer, 1990) pp. 101–115.

[102] J. E. Robinson, Thermoelectric power in the nearly-free-electron model, *Physical Review* **161**, 533 (1967).

[103] A. Feldhoff and B. Geppert, A high-temperature thermoelectric generator based on oxides, *Energy Harvesting and Systems* **1**, 69 (2014).

[104] E. Antončík, On the theory of temperature shift of the absorption curve in non-polar crystals, *Cechoslovackij fiziceskij zurnal* **5**, 449 (1955).

[105] P. Lautenschlager, P. Allen, and M. Cardona, Phonon-induced lifetime broadenings of electronic states and critical points in Si and Ge, *Physical Review B* **33**, 5501 (1986).

[106] F. Giustino, Electron-phonon interactions from first principles, *Reviews of Modern Physics* **89**, 015003 (2017).

[107] P. Keating, Dielectric screening and the phonon spectra of metallic and nonmetallic crystals, *Physical Review* **175**, 1171 (1968).

[108] A. Marini, S. Poncé, and X. Gonze, Many-body perturbation theory approach to the electron-phonon interaction with density-functional theory as a starting point, *Physical Review B* **91**, 224310 (2015).

[109] G. Baym, Field-theoretic approach to the properties of the solid state, *Annals of Physics* **14**, 1 (1961).

[110] L. Hedin and S. Lundqvist, Effects of electron-electron and electron-phonon interactions on the one-electron states of solids, in *Solid State Physics*, Vol. 23 (Elsevier, 1970) pp. 1–181.

- [111] G. Grimvall, *The electron-phonon interaction in metals* (North-Holland, Amsterdam, 1981).
- [112] A. Migdal, Interaction between electrons and lattice vibrations in a normal metal, Sov. Phys. JETP **7**, 996 (1958).
- [113] P. B. Allen and B. Mitrović, Theory of superconducting  $T_c$ , Solid state physics **37**, 1 (1983).
- [114] W. Li, Electrical transport limited by electron-phonon coupling from boltzmann transport equation: An *ab initio* study of Si, Al, and MoS<sub>2</sub>, Physical Review B **92**, 075405 (2015).
- [115] J. I. Mustafa, M. Bernardi, J. B. Neaton, and S. G. Louie, *Ab initio* electronic relaxation times and transport in noble metals, Physical Review B **94**, 155105 (2016).
- [116] X. Gonze and C. Lee, Dynamical matrices, Born effective charges, dielectric permittivity tensors, and interatomic force constants from density-functional perturbation theory, Physical Review B **55**, 10355 (1997).
- [117] C. Verdi and F. Giustino, Fröhlich electron-phonon vertex from first principles, Physical Review Letters **115**, 176401 (2015).
- [118] M. Born and K. Huang, *Dynamical theory of crystal lattices* (Oxford University Press, London, 1954).
- [119] H. Frölich, Electrical breakdown in solid crystals, in *Proc. Roy. Soc.*, Vol. 160 (1937) pp. 230–238.
- [120] H. B. Callen, Electric breakdown in ionic crystals, Physical Review **76**, 1394 (1949).
- [121] D. Howarth and E. Sondheimer, The theory of electronic conduction in polar semi-conductors, Proc. R. Soc. Lond. A **219**, 53 (1953).
- [122] P. Vogl, Microscopic theory of electron-phonon interaction in insulators or semiconductors, Physical Review B **13**, 694 (1976).
- [123] P. Lawaetz, Long-wavelength phonon scattering in nonpolar semiconductors, Physical Review **183**, 730 (1969).
- [124] M. Rohlfing and S. G. Louie, Electron-hole excitations and optical spectra from first principles, Phys. Rev. B **62**, 4927 (2000).
- [125] J. Sjakste, N. Vast, M. Calandra, and F. Mauri, Wannier interpolation of the electron-phonon matrix elements in polar semiconductors: Polar-optical coupling in gaas, Physical Review B **92**, 054307 (2015).
- [126] G. Brunin, H. P. C. Miranda, M. Giantomassi, M. Royo, M. Stengel, M. J. Verstraete, X. Gonze, G.-M. Rignanese, and G. Hautier, Electron-phonon beyond Fröhlich: Dynamical

quadrupoles in polar and covalent solids, *Physical Review Letters* **125**, 136601 (2020).

[127] V. A. Jhalani, J.-J. Zhou, J. Park, C. E. Dreyer, and M. Bernardi, Piezoelectric electron-phonon interaction from *ab initio* dynamical quadrupoles: Impact on charge transport in wurtzite GaN, *Physical Review Letters* **125**, 136602 (2020).

[128] J. Park, J.-J. Zhou, V. A. Jhalani, C. E. Dreyer, and M. Bernardi, Long-range quadrupole electron-phonon interaction from first principles, *Physical Review B* **102**, 125203 (2020).

[129] R. M. Martin, Piezoelectricity, *Physical Review B* **5**, 1607 (1972).

[130] Q. Ren, C. Fu, Q. Qiu, S. Dai, Z. Liu, T. Masuda, S. Asai, M. Hagihala, S. Lee, S. Torri, T. Kamiyama, L. He, X. Tong, C. Felser, D. J. Singh, T. Zhu, J. Yang, and J. Ma, Establishing the carrier scattering phase diagram for ZrNiSn-based half-Heusler thermoelectric materials, *Nature communications* **11**, 1 (2020).

[131] F. Macheda, P. Barone, and F. Mauri, Electron-phonon interaction and longitudinal-transverse phonon splitting in doped semiconductors, *Physical Review Letters* **129**, 185902 (2022).

[132] H. Ehrenreich, Screening effects in polar semiconductors, *Journal of Physics and Chemistry of Solids* **8**, 130 (1959).

[133] A. S. Chaves, D. T. Larson, E. Kaxiras, and A. Antonelli, Microscopic origin of the high thermoelectric figure of merit of n-doped SnSe, *Physical Review B* **104**, 115204 (2021).

[134] A. S. Chaves, D. T. Larson, E. Kaxiras, and A. Antonelli, Out-of-plane thermoelectric performance for p-doped GeSe, *Physical Review B* **105**, 205201 (2022).

[135] B. Radisavljevic and A. Kis, Mobility engineering and a metal–insulator transition in monolayer MoS<sub>2</sub>, *Nature Materials* **12**, 815 (2013).

[136] S.-L. Li, K. Tsukagoshi, E. Orgiu, and P. Samorì, Charge transport and mobility engineering in two-dimensional transition metal chalcogenide semiconductors, *Chemical Society Reviews* **45**, 118 (2016).

[137] G. Bergmann, Weak localization in thin films: a time-of-flight experiment with conduction electrons, *Physics Reports* **107**, 1 (1984).

[138] P. A. Lee and A. D. Stone, Universal conductance fluctuations in metals, *Physical Review Letters* **55**, 1622 (1985).

[139] S. Datta, *Electronic transport in mesoscopic systems* (Cambridge University Press, 1997).

[140] A. Dewandre, O. Hellman, S. Bhattacharya, A. H. Romero, G. K. Madsen, and M. J. Verstraete, Two-step phase transition in SnSe and the origins of its high power factor from first principles, [Physical Review Letters](#) **117**, 276601 (2016).

[141] D. Gunlycke and C. T. White, Graphene valley filter using a line defect, [Physical Review Letters](#) **106**, 136806 (2011).

[142] P. M. Koenraad and M. E. Flatté, Single dopants in semiconductors, [Nature Materials](#) **10**, 91 (2011).

[143] Y. Zheng, T. J. Slade, L. Hu, X. Y. Tan, Y. Luo, Z.-Z. Luo, J. Xu, Q. Yan, and M. G. Kanatzidis, Defect engineering in thermoelectric materials: what have we learned?, [Chemical Society Reviews](#) [10.1039/D1CS00347J](#) (2021).

[144] H. Brooks, Theory of the electrical properties of germanium and silicon, in *Advances in electronics and electron physics*, Vol. 7 (Elsevier, 1955) pp. 85–182.

[145] D. Chatopadhyay and H. J. Queisser, Electron scattering by ionized impurities in semiconductors, [Reviews of Modern Physics](#) **53**, 745 (1981).

[146] E. J. Moore, Quantum-transport theories and multiple scattering in doped semiconductors. I. formal theory, [Physical Review](#) **160**, 607 (1967).

[147] N. Papanikolaou, R. Zeller, P. Dederichs, and N. Stefanou, Lattice distortion in Cu-based dilute alloys: A first-principles study by the KKR Green-function method, [Physical Review B](#) **55**, 4157 (1997).

[148] A. Settels, T. Korhonen, N. Papanikolaou, R. Zeller, and P. Dederichs, *Ab initio* study of acceptor-donor complexes in silicon and germanium, [Physical Review Letters](#) **83**, 4369 (1999).

[149] H. Höhler, N. Atodiresei, K. Schroeder, R. Zeller, and P. Dederichs, Cd-vacancy and Cd-interstitial complexes in Si and Ge, [Physical Review B](#) **70**, 155313 (2004).

[150] H. Ebert, D. Koedderitzsch, and J. Minar, Calculating condensed matter properties using the KKR-Green's function method—recent developments and applications, [Reports on Progress in Physics](#) **74**, 096501 (2011).

[151] O. Restrepo, K. Varga, and S. Pantelides, First-principles calculations of electron mobilities in silicon: Phonon and coulomb scattering, [Applied Physics Letters](#) **94**, 212103 (2009).

[152] V. Lordi, P. Erhart, and D. Åberg, Charge carrier scattering by defects in semiconductors, [Physical Review B](#) **81**, 235204 (2010).

[153] I.-T. Lu, J.-J. Zhou, and M. Bernardi, Efficient *ab initio* calculations of electron-defect scattering and defect-limited carrier mobility, *Physical Review Materials* **3**, 033804 (2019).

[154] I.-T. Lu, J. Park, J.-J. Zhou, and M. Bernardi, *Ab initio* electron-defect interactions using Wannier functions, *npj Computational Materials* **6**, 1 (2020).

[155] A. Cepellotti, J. Coulter, A. Johansson, N. S. Fedorova, and B. Kozinsky, Phoebe: a high-performance framework for solving phonon and electron boltzmann transport equations, *Journal of Physics: Materials* **5**, 035003 (2022).

[156] B. Liao, B. Qiu, J. Zhou, S. Huberman, K. Esfarjani, and G. Chen, Significant reduction of lattice thermal conductivity by the electron-phonon interaction in silicon with high carrier concentrations: A first-principles study, *Physical Review Letters* **114**, 115901 (2015).

[157] J. Garg, N. Bonini, B. Kozinsky, and N. Marzari, Role of disorder and anharmonicity in the thermal conductivity of silicon-germanium alloys: A first-principles study, *Physical Review Letters* **106**, 045901 (2011).

[158] W. Li, J. Carrete, N. A. Katcho, and N. Mingo, ShengBTE: a solver of the Boltzmann transport equation for phonons, *Comp. Phys. Commun.* **185**, 1747–1758 (2014).

[159] G. K. Madsen and D. J. Singh, Boltztrap. a code for calculating band-structure dependent quantities, *Computer Physics Communications* **175**, 67 (2006).

[160] J. Bardeen and W. Shockley, Deformation potentials and mobilities in non-polar crystals, *Physical Review* **80**, 72 (1950).

[161] J. Xi, M. Long, L. Tang, D. Wang, and Z. Shuai, First-principles prediction of charge mobility in carbon and organic nanomaterials, *Nanoscale* **4**, 4348 (2012).

[162] L. Xi, S. Pan, X. Li, Y. Xu, J. Ni, X. Sun, J. Yang, J. Luo, J. Xi, W. Zhu, *et al.*, Discovery of high-performance thermoelectric chalcogenides through reliable high-throughput material screening, *Journal of the American Chemical Society* **140**, 10785 (2018).

[163] A. M. Ganose, J. Park, A. Faghaninia, R. Woods-Robinson, K. A. Persson, and A. Jain, Efficient calculation of carrier scattering rates from first principles, *Nature communications* **12**, 1 (2021).

[164] J. Ma, A. S. Nessimagoudar, and W. Li, First-principles study of electron and hole mobilities of Si and GaAs, *Physical Review B* **97**, 045201 (2018).

[165] F. Giustino, M. L. Cohen, and S. G. Louie, Electron-phonon interaction using Wannier functions, *Physical Review B* **76**, 165108 (2007).

[166] L. A. Agapito and M. Bernardi, *Ab initio* electron-phonon interactions using atomic orbital wave functions, *Physical Review B* **97**, 10.1103/PhysRevB.97.235146 (2018).

[167] G. Samsonidze and B. Kozinsky, Accelerated screening of thermoelectric materials by first-principles computations of electron–phonon scattering, *Advanced Energy Materials* **8**, 1800246 (2018).

[168] T. Deng, G. Wu, M. B. Sullivan, Z. M. Wong, K. Hippalgaonkar, J.-S. Wang, and S.-W. Yang, EPIC STAR: a reliable and efficient approach for phonon-and impurity-limited charge transport calculations, *npj Computational Materials* **6**, 1 (2020).

[169] M. Yao, Y. Wang, X. Li, Y. Sheng, H. Huo, L. Xi, J. Yang, and W. Zhang, Materials informatics platform with three dimensional structures, workflow and thermoelectric applications, *Scientific Data* **8**, 1 (2021).

[170] S. Poncé, E. R. Margine, C. Verdi, and F. Giustino, Epw: Electron–phonon coupling, transport and superconducting properties using maximally localized wannier functions, *Computer Physics Communications* **209**, 116 (2016).

[171] J.-J. Zhou, J. Park, I.-T. Lu, I. Maliyov, X. Tong, and M. Bernardi, Perturbo: A software package for *ab initio* electron–phonon interactions, charge transport and ultrafast dynamics, *Computer Physics Communications* **264**, 107970 (2021).

[172] C. Brouder, G. Panati, M. Calandra, C. Mourougane, and N. Marzari, Exponential localization of Wannier functions in insulators, *Physical Review Letters* **98**, 046402 (2007).

[173] I. Souza, N. Marzari, and D. Vanderbilt, Maximally localized Wannier functions for entangled energy bands, *Physical Review B* **65**, 035109 (2001).

[174] A. L. Fetter and J. D. Walecka, *Quantum theory of many-particle systems* (Courier Corporation, 2012).

[175] A. S. Chaves, A. Antonelli, D. T. Larson, and E. Kaxiras, Boosting the efficiency of *ab initio* electron-phonon coupling calculations through dual interpolation, *Physical Review B* **102**, 125116 (2020).

[176] D. J. Chadi and M. L. Cohen, Special points in the Brillouin zone, *Physical Review B* **8**, 5747 (1973).

[177] D. G. Shankland, Interpolation in k-space with functions of arbitrary smoothness, in *Computational Methods in Band Theory* (Springer, 1971) pp. 362–367.

[178] D. Koelling and J. Wood, On the interpolation of eigenvalues and a resultant integration scheme, *Journal of Computational Physics* **67**, 253 (1986).

[179] W. E. Pickett, H. Krakauer, and P. B. Allen, Smooth fourier interpolation of periodic functions, *Physical Review B* **38**, 2721 (1988).

[180] A. Togo, L. Chaput, and I. Tanaka, Distributions of phonon lifetimes in brillouin zones, *Phys. Rev. B* **91**, 094306 (2015).

[181] J. Carrete, N. Mingo, and S. Curtarolo, Low thermal conductivity and triaxial phononic anisotropy of SnSe, *Applied Physics Letters* **105**, 101907 (2014).

[182] Y. Pei, X. Shi, A. LaLonde, H. Wang, L. Chen, and G. J. Snyder, Convergence of electronic bands for high performance bulk thermoelectrics, *Nature* **473**, 66 (2011).

[183] Y. Pei, H. Wang, and G. J. Snyder, Band engineering of thermoelectric materials, *Advanced Materials* **24**, 6125 (2012).

[184] W. Liu, X. Tan, K. Yin, H. Liu, X. Tang, J. Shi, Q. Zhang, and C. Uher, Convergence of conduction bands as a means of enhancing thermoelectric performance of n-type  $Mg_2Si_{1-x}Sn_x$  solid solutions, *Physical Review Letters* **108**, 166601 (2012).

[185] A. M. Dehkordi, M. Zebarjadi, J. He, and T. M. Tritt, Thermoelectric power factor: Enhancement mechanisms and strategies for higher performance thermoelectric materials, *Materials Science and Engineering: R: Reports* **97**, 1 (2015).

[186] D. S. Parker, A. F. May, and D. J. Singh, Benefits of carrier-pocket anisotropy to thermoelectric performance: The case of p-type  $AgBiSe_2$ , *Physical Review Applied* **3**, 064003 (2015).

[187] D. Morelli, V. Jovovic, and J. Heremans, Intrinsically minimal thermal conductivity in cubic I-VI<sub>2</sub> semiconductors, *Physical Review Letters* **101**, 035901 (2008).

[188] J. He, M. Amsler, Y. Xia, S. S. Naghavi, V. I. Hegde, S. Hao, S. Goedecker, V. Ozolinš, and C. Wolverton, Ultralow thermal conductivity in full heusler semiconductors, *Physical Review Letters* **117**, 046602 (2016).

[189] R. L. González-Romero, A. Antonelli, A. S. Chaves, and J. J. Meléndez, Ultralow and anisotropic thermal conductivity in semiconductor  $As_2Se_3$ , *Physical Chemistry Chemical Physics* **20**, 1809 (2018).

[190] A. I. Hochbaum, R. Chen, R. D. Delgado, W. Liang, E. C. Garnett, M. Najarian, A. Majumdar, and P. Yang, Enhanced thermoelectric performance of rough silicon nanowires, *Nature*

**451**, 163 (2008).

- [191] A. I. Boukai, Y. Bunimovich, J. Tahir-Kheli, J.-K. Yu, W. A. Goddard III, and J. R. Heath, Silicon nanowires as efficient thermoelectric materials, *Nature* **451**, 168 (2008).
- [192] M. G. Kanatzidis, Nanostructured thermoelectrics: the new paradigm?, *Chemistry of Materials* **22**, 648 (2009).
- [193] L.-D. Zhao, S. Hao, S.-H. Lo, C.-I. Wu, X. Zhou, Y. Lee, H. Li, K. Biswas, T. P. Hogan, C. Uher, C. Wolverton, V. P. Dravid, and K. M. G, High thermoelectric performance via hierarchical compositionally alloyed nanostructures, *Journal of the American Chemical Society* **135**, 7364 (2013).
- [194] R. W. McKinney, P. Gorai, V. Stevanović, and E. S. Toberer, Search for new thermoelectric materials with low Lorenz number, *Journal of Materials Chemistry A* **5**, 17302 (2017).
- [195] G. Mahan and J. Sofo, The best thermoelectric, *Proceedings of the National Academy of Sciences* **93**, 7436 (1996).
- [196] L. L. Baranowski, G. Jeffrey Snyder, and E. S. Toberer, Effective thermal conductivity in thermoelectric materials, *Journal of Applied Physics* **113**, 204904 (2013).
- [197] B. R. Ortiz, P. Gorai, L. Krishna, R. Mow, A. Lopez, R. McKinney, V. Stevanović, and E. S. Toberer, Potential for high thermoelectric performance in n-type Zintl compounds: a case study of Ba doped KAlSb<sub>4</sub>, *Journal of Materials Chemistry A* **5**, 4036 (2017).
- [198] A. Putatunda and D. J. Singh, Lorenz number in relation to estimates based on the Seebeck coefficient, *Materials Today Physics* **8**, 49 (2019).
- [199] J. He and T. M. Tritt, Advances in thermoelectric materials research: Looking back and moving forward, *Science* **357**, eaak9997 (2017).
- [200] K. Biswas, J. He, I. D. Blum, C.-I. Wu, T. P. Hogan, D. N. Seidman, V. P. Dravid, and M. G. Kanatzidis, High-performance bulk thermoelectrics with all-scale hierarchical architectures, *Nature* **489**, 414 (2012).
- [201] H. Liu, X. Shi, F. Xu, L. Zhang, W. Zhang, L. Chen, Q. Li, C. Uher, T. Day, and G. J. Snyder, Copper ion liquid-like thermoelectrics, *Nature Materials* **11**, 422 (2012).
- [202] T. Fu, X. Yue, H. Wu, C. Fu, T. Zhu, X. Liu, L. Hu, P. Ying, J. He, and X. Zhao, Enhanced thermoelectric performance of PbTe bulk materials with figure of merit  $zT > 2$  by multi-functional alloying, *Journal of Materomics* **2**, 141 (2016).

[203] A. Olvera, N. Moroz, P. Sahoo, P. Ren, T. Bailey, A. Page, C. Uher, and P. Poudeu, Partial indium solubility induces chemical stability and colossal thermoelectric figure of merit in Cu<sub>2</sub>Se, *Energy & Environmental Science* **10**, 1668 (2017).

[204] Y. Cheng, J. Yang, Q. Jiang, D. He, J. He, Y. Luo, D. Zhang, Z. Zhou, Y. Ren, and J. Xin, New insight into InSb-based thermoelectric materials: from a divorced eutectic design to a remarkably high thermoelectric performance, *Journal of Materials Chemistry A* **5**, 5163 (2017).

[205] N. Ma, Y.-Y. Li, L. Chen, and L.-M. Wu,  $\alpha$ -CsCu<sub>5</sub>Se<sub>3</sub>: discovery of a low-cost bulk selenide with high thermoelectric performance, *Journal of the American Chemical Society* **142**, 5293 (2020).

[206] S. Roychowdhury, T. Ghosh, R. Arora, M. Samanta, L. Xie, N. K. Singh, A. Soni, J. He, U. V. Waghmare, and K. Biswas, Enhanced atomic ordering leads to high thermoelectric performance in AgSbTe<sub>2</sub>, *Science* **371**, 722 (2021).

[207] I. Terasaki, Y. Sasago, and K. Uchinokura, Large thermoelectric power in NaCo<sub>2</sub>O<sub>4</sub> single crystals, *Physical Review B* **56**, R12685 (1997).

[208] J.-S. Rhyee, K. H. Lee, S. M. Lee, E. Cho, S. I. Kim, E. Lee, Y. S. Kwon, J. H. Shim, and G. Kotliar, Peierls distortion as a route to high thermoelectric performance in In<sub>4</sub>Se<sub>3- $\delta$</sub>  crystals, *Nature* **459**, 965 (2009).

[209] H. Ohta, S. W. Kim, S. Kaneki, A. Yamamoto, and T. Hashizume, High thermoelectric power factor of high-mobility 2d electron gas, *Advanced Science* **5**, 1700696 (2018).

[210] L. Cheng, C. Zhang, and Y. Liu, The optimal electronic structure for high-mobility 2D semiconductors: exceptionally high hole mobility in 2D antimony, *Journal of the American Chemical Society* **141**, 16296 (2019).

[211] Z. Li, C. Xiao, and Y. Xie, Layered thermoelectric materials: Structure, bonding, and performance mechanisms, *Applied Physics Reviews* **9**, 011303 (2022).

[212] L.-D. Zhao, S.-H. Lo, Y. Zhang, H. Sun, G. Tan, C. Uher, C. Wolverton, V. P. Dravid, and M. G. Kanatzidis, Ultralow thermal conductivity and high thermoelectric figure of merit in SnSe crystals, *Nature* **508**, 373 (2014).

[213] L.-D. Zhao, G. Tan, S. Hao, J. He, Y. Pei, H. Chi, H. Wang, S. Gong, H. Xu, V. P. Dravid, *et al.*, Ultrahigh power factor and thermoelectric performance in hole-doped single-crystal SnSe, *Science* **351**, 141 (2016).

[214] C. Chang, M. Wu, D. He, Y. Pei, C.-F. Wu, X. Wu, H. Yu, F. Zhu, K. Wang, Y. Chen, *et al.*, 3D charge and 2D phonon transports leading to high out-of-plane ZT in n-type SnSe crystals, [Science 360, 778 \(2018\)](#).

[215] G. Ding, G. Gao, and K. Yao, High-efficient thermoelectric materials: The case of orthorhombic IV-VI compounds, [Scientific reports 5, 1 \(2015\)](#).

[216] R. Guo, X. Wang, Y. Kuang, and B. Huang, First-principles study of anisotropic thermoelectric transport properties of IV-VI semiconductor compounds SnSe and SnS, [Physical Review B 92, 115202 \(2015\)](#).

[217] J. M. Skelton, L. A. Burton, S. C. Parker, A. Walsh, C.-E. Kim, A. Soon, J. Buckeridge, A. A. Sokol, C. R. A. Catlow, A. Togo, *et al.*, Anharmonicity in the high-temperature Cmcm phase of SnSe: Soft modes and three-phonon interactions, [Physical Review Letters 117, 075502 \(2016\)](#).

[218] S. Li, Z. Tong, and H. Bao, Resolving different scattering effects on the thermal and electrical transport in doped SnSe, [Journal of Applied Physics 126, 025111 \(2019\)](#).

[219] U. Aseginolaza, R. Bianco, L. Monacelli, L. Paulatto, M. Calandra, F. Mauri, A. Bergara, and I. Errea, Phonon collapse and second-order phase transition in thermoelectric SnSe, [Physical Review Letters 122, 075901 \(2019\)](#).

[220] X. Zhang, J. Shen, S. Lin, J. Li, Z. Chen, W. Li, and Y. Pei, Thermoelectric properties of GeSe, [Journal of Materomics 2, 331 \(2016\)](#).

[221] L. Shaabani, S. Aminorroaya-Yamini, J. Byrnes, A. Akbar Nezhad, and G. R. Blake, Thermoelectric performance of Na-doped GeSe, [ACS omega 2, 9192 \(2017\)](#).

[222] S. Hao, F. Shi, V. P. Dravid, M. G. Kanatzidis, and C. Wolverton, Computational prediction of high thermoelectric performance in hole doped layered GeSe, [Chemistry of Materials 28, 3218 \(2016\)](#).

[223] S. Roychowdhury, M. Samanta, S. Perumal, and K. Biswas, Germanium chalcogenide thermoelectrics: electronic structure modulation and low lattice thermal conductivity, [Chemistry of Materials 30, 5799 \(2018\)](#).

[224] K. Yuan, Z. Sun, X. Zhang, and D. Tang, Tailoring phononic, electronic, and thermoelectric properties of orthorhombic GeSe through hydrostatic pressure, [Scientific reports 9, 1 \(2019\)](#).

[225] M. Asen-Palmer, K. Bartkowiak, E. Gmelin, M. Cardona, A. Zhernov, A. Inyushkin, A. Taldenkov, V. Ozhogin, K. M. Itoh, and E. Haller, Thermal conductivity of germanium

crystals with different isotopic compositions, *Physical Review B* **56**, 9431 (1997).

[226] M. Omini and A. Sparavigna, An iterative approach to the phonon boltzmann equation in the theory of thermal conductivity, *Physica B: Condensed Matter* **212**, 101 (1995).

[227] M. Simoncelli, N. Marzari, and F. Mauri, Unified theory of thermal transport in crystals and glasses, *Nature Physics* **15**, 809 (2019).

[228] C. Zhou, Y. K. Lee, Y. Yu, S. Byun, Z.-Z. Luo, H. Lee, B. Ge, Y.-L. Lee, X. Chen, J. Y. Lee, *et al.*, Polycrystalline SnSe with a thermoelectric figure of merit greater than the single crystal, *Nature Materials* **20**, 1378 (2021).

[229] D. Ibrahim, J.-B. Vaney, S. Sassi, C. Candolfi, V. Ohorodniichuk, P. Levinsky, C. Semprimoschnig, A. Dauscher, and B. Lenoir, Reinvestigation of the thermal properties of single-crystalline SnSe, *Applied Physics Letters* **110**, 032103 (2017).

[230] D. Sarkar, T. Ghosh, S. Roychowdhury, R. Arora, S. Sajan, G. Sheet, U. V. Waghmare, and K. Biswas, Ferroelectric instability induced ultralow thermal conductivity and high thermoelectric performance in rhombohedral p-type GeSe crystal, *Journal of the American Chemical Society* **142**, 12237 (2020).

[231] Y. Xia, Revisiting lattice thermal transport in PbTe: The crucial role of quartic anharmonicity, *Applied Physics Letters* **113**, 073901 (2018).

[232] P.-C. Wei, S. Bhattacharya, J. He, S. Neeleshwar, R. Podila, Y. Chen, and A. Rao, The intrinsic thermal conductivity of SnSe, *Nature* **539**, E1 (2016).

[233] L.-D. Zhao, S.-H. Lo, Y. Zhang, H. Sun, G. Tan, C. Uher, C. Wolverton, V. P. Dravid, and M. G. Kanatzidis, The intrinsic thermal conductivity of SnSe: Reply, *Nature* **539**, E2 (2016).

[234] D. Wu, L. Wu, D. He, L.-D. Zhao, W. Li, M. Wu, M. Jin, J. Xu, J. Jiang, L. Huang, *et al.*, Direct observation of vast off-stoichiometric defects in single crystalline SnSe, *Nano Energy* **35**, 321 (2017).

[235] Y. K. Lee, Z. Luo, S. P. Cho, M. G. Kanatzidis, and I. Chung, Surface oxide removal for polycrystalline SnSe reveals near-single-crystal thermoelectric performance, *Joule* **3**, 719 (2019).